ISSN 2767-6641 (Online)
Volume 2 I Issue 3 I September 2021

Extracellular Vesicles and Circulating Nucleic Acids

evcna

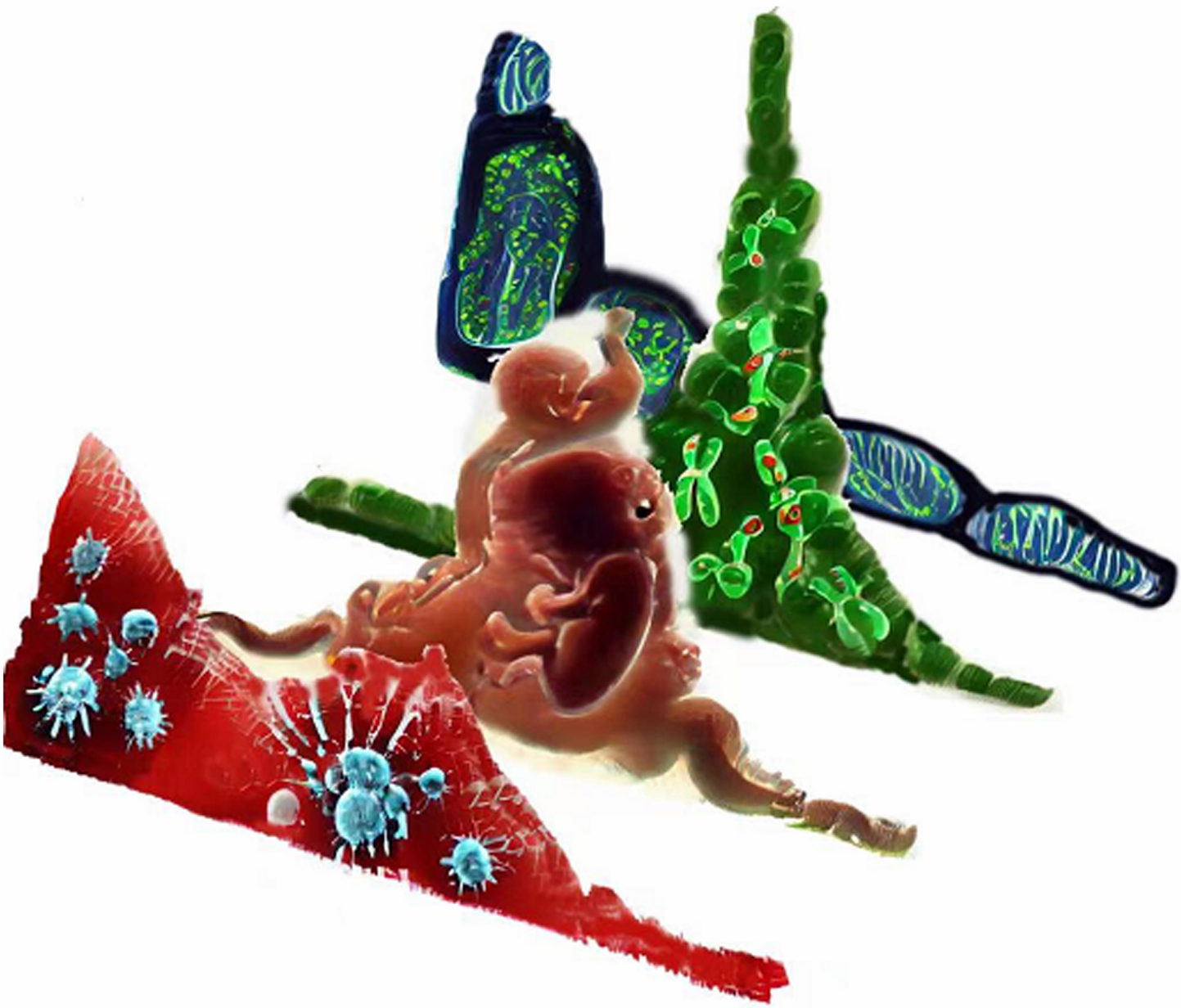

Open Access

www.evcna.com

EDITORIAL BOARD

GENERAL INFORMATION

About the Journal

Extracellular Vesicles and Circulating Nucleic Acids (*EVCNA*), is an international, peer-reviewed, open access journal. *Extracellular Vesicles and Circulating Nucleic Acids* provides an online platform for the sharing of research data, new methodology, reviews and commentaries in the areas of extracellular vesicles and circulating nucleic acids including DNA, RNA, and miRNA and their therapeutic use. The journal is committed to the rapid publication of original findings that increase our understanding of the molecular and cell biology, biogenesis, and origin of extracellular vesicles and circulating nucleic acids; and their use as biomarkers for the diagnosis, prognostication and surveillance of disease states, and in therapeutics. Manuscripts with clinical relevance are especially encouraged to promote the translation from basic science to clinical applications. The criteria for acceptance are scientific excellence and originality. All works involving the use of animals and human subjects must have been approved by institutional review committees and adhere to accepted international ethical standards.

Information for Authors

Manuscripts should be prepared in accordance with Author Instructions.
Please check www.evcnajournal.com/pages/view/author_instructions for details.
All manuscripts should be submitted online at https://oaemesas.com/login?JournalId=evcna.

Copyright

Permissions

For information on how to request permissions to reproduce articles/information from this journal, please visit www.evcnajournal.com.

Disclaimer

The information and opinions presented in the journal reflect the views of the authors and not of the journal or its Editorial Board or the Publisher. Publication does not constitute endorsement by the journal. Neither the *EVCNA* nor its publishers nor anyone else involved in creating, producing or delivering the *EVCNA* or the materials contained therein, assumes any liability or responsibility for the accuracy, completeness, or usefulness of any information provided in the *EVCNA*, nor shall they be liable for any direct, indirect, incidental, special, consequential or punitive damages arising out of the use of the *EVCNA*. The *EVCNA*, nor its publishers, nor any other party involved in the preparation of material contained in the *EVCNA* represents or warrants that the information contained herein is in every respect accurate or complete, and they are not responsible for any errors or omissions or for the results obtained from the use of such material. Readers are encouraged to confirm the information contained herein with other sources.

Publisher

OAE Publishing Inc.
245 E Main Street st112, Alhambra, CA 91801, USA
Website: www.oaepublish.com

Contacts

E-mail: editorialoffice@evcnajournal.com
Website: www.evcnajournal.com

Extracellular Vesicles and Circulating Nucleic Acids

CONTENTS

Volume 2 / Issue 3 / September 2021

Ragni *et al. Extracell Vesicles Circ Nucleic Acids* 2021;2:202-21
DOI: 10.20517/evcna.2021.11

Extracellular Vesicles and Circulating Nucleic Acids

Original Article

Open Access

Check for updates

Comparison of miRNA cargo in human adipose-tissue *vs.* amniotic-membrane derived mesenchymal stromal cells extracellular vesicles for osteoarthritis treatment

Enrico Ragni[1,*], Carlotta Perucca Orfei[1], Andrea Papait[2,3], Laura de Girolamo[1]

[1]IRCCS Istituto Ortopedico Galeazzi, Laboratorio di Biotecnologie Applicate all' Ortopedia, Milan I-20161, Italy.
[2]Centro di Ricerca E. Menni, Fondazione Poliambulanza Istituto Ospedaliero, Brescia I-25124, Italy.
[3]Department of Life Science and Public Health, Università Cattolica del Sacro Cuore, Rome I-00168, Italy.

Correspondence to: Dr. Enrico Ragni, IRCCS Istituto Ortopedico Galeazzi, Laboratorio di Biotecnologie Applicate all' Ortopedia, Via R. Galeazzi 4, Milan I-20161, Italy. E-mail: enrico.ragni@grupposandonato.it

How to cite this article: Ragni E, Perucca Orfei C, Papait A, de Girolamo L. Comparison of miRNA cargo in human adipose-tissue *vs.* amniotic-membrane derived mesenchymal stromal cells extracellular vesicles for osteoarthritis treatment. *Extracell Vesicles Circ Nucleic Acids* 2021;2:202-21. https://dx.doi.org/10.20517/evcna.2021.11

Received: 30 Jun 2021 **First Decision:** 21 Jul 2021 **Revised:** 27 Jul 2021 **Accepted:** 30 Jul 2021 **First online:** 3 Aug 2021

Academic Editors: Yoke Peng Loh, Tsuneya Ikezu **Copy Editor:** Yue-Yue Zhang **Production Editor:** Yue-Yue Zhang

Abstract

Aim: Mesenchymal stromal cells (MSCs) emerged as a promising therapeutic option for osteoarthritis (OA) management, in particular those isolated from adipose tissue (hASCs) and amniotic membrane (hAMSCs). The cartilage protective and immunomodulatory features of hASCs and hAMSCs are ascribed to secreted factors, including extracellular vesicles (EVs) and embedded miRNAs. The purpose of this study was to compare EVs and shuttled miRNAs from both MSC types and discuss them in the frame of OA pathological tissues.

Methods: Human hASCs and hAMSCs were analyzed by flow cytometry. EVs were analyzed by flow cytometry, nanoparticle tracking analysis, and electron microscopy. High-throughput qRT-PCR miRNA data available in the literature were compared. Abundant miRNAs and their experimentally validated targets were associated with those reported to drive OA pathology at cartilage, synovia, and macrophage levels. Four tools (Genorm, Normfinder, BestKeeper, and Delta Ct) were used to identify EVs stable reference genes.

Results: EVs did not show phenotypical or dimensional differences between the two sources, with hAMSCs releasing more particles. In total, 307 EV miRNAs were identified, with 306 shared. Several of the most abundant miRNAs target OA-driving factors and are involved in cartilage and synovia protective mechanisms, with hAMSC-EVs' preponderance for M2 anti-inflammatory macrophage commitment. miR-34a-5p emerged as the most stable reference gene.

Conclusion: Both hASCs and hAMSCs release EVs enriched in joint-protective and anti-inflammatory miRNAs, supporting their use for treatment of joint diseases. Future comparative clinical studies would be needed to test whether hAMSCs' higher EV secretion and enhanced M2 macrophage polarizing miRNA cargo allow for potentially increased OA therapeutic features.

Keywords: Extracellular vesicles, miRNAs, mesenchymal stromal cells, adipose tissue, amniotic membrane, osteoarthritis, joint diseases, regenerative medicine

INTRODUCTION

Osteoarthritis (OA) is a common progressive multifactorial joint disease affecting 7% of the global population and one of the leading causes of disability in older adults[1]. OA pathogenesis involves mechanical, inflammatory, and metabolic factors, eventually leading to an imbalance between the repair and destruction of joint tissues, such as cartilage and synovium[2]. Chondrocytes in the damaged cartilage enhance extracellular matrix degradation and released products, together with pro-inflammatory mediators, act on synoviocytes and inflammatory cells of the synovium, stimulating pro-inflammatory responses[2]. To date, early-stage treatments, such as pharmacological methods, address OA symptoms by reducing inflammation and pain[3]. Consequently, these conservative approaches are not effective in disease amelioration but only postpone the need of joint replacement, opening the search for novel and biological therapeutic strategies.

In this scenario, mesenchymal stromal cell (MSC)-based treatments emerged as a promising new approach for OA[4]. MSCs are multipotent cells that can be found in many different stromal tissues, both adult and perinatal. MSCs, in the case of injury or disease, secrete bioactive factors, both free as cytokines/chemokines and embedded in extracellular vesicles (EVs) as miRNAs, with immunomodulatory and trophic functions[5]. Human adipose tissue/stromal vascular fraction (SVF) and amniotic membrane (AM) have gained particular attention as tissue sources for MSCs, and, despite their different origins, they share some crucial advantages. Both sources can be easily harvested without ethical controversy since they are obtained from biological waste after liposuction or birth, respectively. In addition, they have a higher cell recovery [1×10^5 human adipose-derived MSCs (hASCs)[6] or 1×10^6 human amniotic membrane-derived MSCs (hAMSCs)[7] per tissue gram][8] with respect to bone marrow [3×10^3 human bone marrow-derived MSCs[9] per mL][10]. Adipose tissue has been largely studied in more than 20 OA-related clinical trials in the form of expanded hASCs[11,12], unprocessed SVF, or micro/nano-fragmented adipose tissue. On the contrary, AM is still in its infancy, with few reported trials using both allogenic hAMSCs[13] and most frequently amniotic suspension allografts[14-16]. Notably, the majority of these clinical studies reported significant improvements in terms of pain and knee function. However, the substantial lack of consistency in terms of treatment protocols and assessment of clinical outcomes prevents an efficient comparison of these data, and therefore it is hard to determine the most effective source of MSCs[17].

Beyond a missing direct clinical comparison of hASCs *vs.* hAMSCs in the clinical OA setting, basic research is also very scarce. In fact, several reviews describe the different MSC types for OA therapy[18], with abundance of *in vitro* and pre-clinical results, but very few data characterizing hASCs *vs.* hAMSCs in the

same study are available. Topoluk *et al.*[19]showed that hAMSCs have a greater differentiation potential toward bone and cartilage compared with hASCs. In addition, in a sophisticated *in vitro* coculture model of patient-matched human OA cartilage and synovium, hAMSCs resulted more chondroprotective and more effective at reducing the OA pro-inflammatory: anti-inflammatory (M1:M2) synovial macrophage ratio[20]. These features might be ascribed to different secretory activity, including EVs and their miRNAs. Consistently, whole secretome and MSC-EVs have been reported to mimic and even surpass MSCs' protective ability in the OA setting, and this was seen for both hAMSCs[21] and hASCs[22-25] whose EVs were reported *in vitro* to polarize macrophages by upregulating the expression of M2 markers[26,27]. This immunomodulatory feature was also recently described for other MSC-EV types, such as embryonic stem cell-, bone marrow-, and Wharton's jelly-derived ones, during cartilage repair in animal models[28-30]. Notably, differences in miRNA cargo were postulated to account for divergent immunomodulatory and trophic properties of EVs from alternative sources[31], although the relevance of these differences have not been discussed for OA.

Thus, the goal of this study was to compare cells, EVs, and embedded miRNA cargo sifting data previously obtained in our laboratory with identical technical approaches and platforms (hASCs[32] and hAMSCs[21]). Whole miRNomes and differentially expressed players were analyzed by bioinformatics for miRNA-mRNA interactions using expression data from OA-affected tissues and cells. These results give the molecular basis for future clinical investigations that directly compare hAMSCs and hASCs within the same study for OA treatment.

METHODS

hASCs and hAMSCs isolation and culture

Adipose tissue was obtained as waste material from three female donors (54 years ± 8 years) who underwent liposuction for aesthetic purposes and gave their consent to donate waste biological material for research purposes. hASCs were isolated as previously described[32]. After selection for plastic adhesion, cells were expanded in DMEM high glucose (Sigma Aldrich, St. Louis, MO, USA) supplemented with FBS (GE Healthcare, Piscataway, NJ, USA) at 37 °C in a humidified atmosphere with 5% CO_2 and used at Passage 3. Human term placentas were collected as waste material from three healthy women. hAMSCs were isolated as previously described[21]. Cells were then expanded in CHANG C medium (Irvine Scientific, Irvine, CA, USA) at 37 °C in a humidified atmosphere with 5% CO_2 and used at Passage 2.

hASCs and hAMSCs characterization by flow cytometry

hASCs and hAMSCs were analyzed with a CytoFLEX flow cytometer (Beckman Coulter, Fullerton, CA, USA), collecting at least 30,000 events. Antibodies were used in two panels: (1) anti-CD44-PE-Vio770 (REA690, Miltenyi Biotec, Bergisch Gladbach, Germany), CD73-PE (REA804, Miltenyi), and CD90-FITC (REA897, Miltenyi); and (2) CD31-PerCP-Vio700 (REA730, Miltenyi), CD34-FITC (AC136, Miltenyi), and CD45-PE-Vio770 (REA747, Miltenyi).

Cell culture supernatant collection

hASCs and hAMSCs at 90% confluence were washed three times with PBS to remove residues of exhausted media, and fresh media without supplements were added at 0.07 mL/cm^2. After 48 h, cells were detached and counted with an automatic cell counter, NucleoCounter NC-3000 (ChemoMetec, Allerod, Denmark), while media were collected and serially centrifuged (376 g, 1000 g, 2000 g, and twice at 4000 g, 15 min each) at 4 °C to eliminate debris, floating cells, and apoptotic bodies.

EVs detection by nanoparticle tracking analysis

EVs in the serially centrifuged supernatant (1:2 diluted in PBS for hASCs and 1:10 diluted for hAMSCs) were visualized by the NanoSight LM10-HS system (NanoSight Ltd, Amesbury, UK). Five 30 s recordings were performed, and the data were analyzed by nanoparticle tracking analysis (NTA) software, providing high-resolution particle size distribution profiles and concentration measurements. The number of EVs per cell for both hASCs and hAMSCs was calculated.

EVs characterization by flow cytometry

NTA data were used to obtain supernatant samples with similar numbers of EVs (approximately 1-2 × 10^6 EVs) in a final volume of 20 μL, either PBS or PBS + 0.1 μM CFSE, and incubation was performed in the dark at 37 °C for 1 h. CFSE-unlabeled samples were stored at 4 °C, whereas CFSE-labeled samples were stained for 30 min at 4 °C in the dark with 1 μL of the following APC-conjugated Abs: anti-CD9 (312107, BioLegend, San Diego, CA, USA), CD63 (353007, BioLegend), CD81 (349509, BioLegend), anti-CD44 (338805, BioLegend), CD73 (344005, BioLegend), and CD90 (328113, BioLegend). Antibodies were used individually after being centrifuged at 16,000 g for 20 min at 4 °C to remove debris. After incubation, PBS to a final volume of 200 μL was added to both stained (CFSE and CFSE + Abs) and unstained samples, and events collection was performed with a CytoFLEX flow cytometer at 10 μL/min flow rate. To identify CFSE positive EVs, a first gate in the FITC channel was performed using unstained EVs as negative samples. FITC + events were used to create APC-positive and -negative gates to visualize in CFSE + Abs-treated samples the EVs harboring the respective antigens. The flow cytometer was previously calibrated with reference Megamix-Plus SSC beads (Biocytex, Marseille, France) composed of FITC fluorescent spheres (160, 200, 240, and 500 nm).

EV characterization by transmission electron microscopy

Thirteen milliliters of serially centrifuged supernatant were 1:2 diluted with PBS and centrifuged at 100,000 g for 9 h at 4 °C in a 70.1Ti rotor (Beckman Coulter, Fullerton, CA, USA). After pellet suspension in PBS (100 μL), 5 μL were absorbed for 10 min at RT on formvar carbon-coated grids and excess liquid removed by filter paper. Uranyl acetate aqueous suspension (2%, 10 min) gave the negative staining and excess liquid was removed by filter paper. Eventually, the grid was dried at RT. Images were acquired with a TALOS L120C transmission electron microscopy (TEM) (Thermo Fisher Scientific, Waltham, MA, USA) at 120 kV.

EV miRNA retrieval and normalization

EV miRNA qRT-PCR data were obtained as previously published[21,32]. Briefly, EV pellets were dissolved in Trizol reagent (Sigma Aldrich) and 6 pg of a nonhuman synthetic miRNA spike-in (Arabidopsis thaliana ath-miR-159a) were added to monitor the technical variability during the whole detection procedure and during subsequent reactions for the eventual equalization of panels A and B of the OpenArray® platform (Thermo Fisher Scientific, Waltham, MA, USA). RNA was extracted with miRNeasy and RNeasy CleanUp Kits to isolate RNA enriched in small molecules < 200 nt (Qiagen, Hilden, Germany), and cDNAs were obtained by standard reverse transcription, with preamplification performed with A and B independent kits, followed by RT-PCR analysis with the QuantStudio™ 12 K Flex OpenArray® Platform (QS12KFlex) on A and B miRNA panels, which together cover 754 human miRNA sequences from the Sanger miRBase v21. Only miRNAs present in all three isolates and shared between hASC-EVs and hAMSC-EVs were considered for normalization, which was performed using the global mean strategy[33]. For the final analysis, miRNAs with STD > 2 in either hASC-EVs or hAMSC-EVs were excluded to avoid strong donor-dependent variability and define a constant tissue-type specific message. The genetic weight was calculated with the ΔC_{RT} method between normalized miRNAs (using the lowest normalized C_{RT} as milestone for ΔC_{RT} calculations between miRNAs), giving an arbitrary value of 1 to the lowest normalized C_{RT} and $2^{-\Delta CRT}$ value

to the following candidates. Thereafter, the sum was calculated and the weight for each miRNA was obtained with the formula: (arbitrary miRNA value/sum of arbitrary values) × 100.

Assessment of miRNA RG stability

miRNA expression stability was evaluated on the molecules lying in the first quartiles of expression according to four gold-standard statistical approaches: geNorm[34], NormFinder[35], BestKeeper[36], and the comparative Delta Ct method[37]. The overall performance of the miRNA RGs was evaluated by a global approach relying on the geometric mean of the rankings given by each analysis obtained with the RefFinder platform[38].

Hierarchical clustering and principal component analysis

Heat maps showing hierarchical clustering and principal component analysis (PCA) plots were generated on normalized C_{RT} values with ClustVis package (https://biit.cs.ut.ee/clustvis/)[39]. The only miRNA expressed in hAMSC-EVs and absent in hASC-EVs was tagged with a C_{RT} value of 30 in hASC-EVs. Data pre-processing for the PCA method included: (1) no transformation; (2) no centering; (3) no scaling applied to rows; and (4) SVD with imputation. Heat map clustering options included: both rows and columns were clustered using correlation distance and average linkage.

EV miRNA target identification

miRTarBase database (https://mirtarbase.cuhk.edu.cn/~miRTarBase/miRTarBase_2019/php/index.php)[40] was used to retrieve the EV miRNA targets, selecting only those interactions reported to be validated by strong experimental evidence (reporter assay, Western blot, and qPCR).

Statistical analysis

Student's two-tailed *t*-test was used to compare cell density values, EV release per cell type, and hASC-EV and hAMSC-EV normalized miRNA C_{RT} values, with *P*-value set at $P < 0.05$ for significance.

RESULTS

Phenotype characterization of hASCs, hAMSCs and secreted EVs

Both hASCs and hAMSCs were simultaneously characterized by flow cytometry for MSC and hematoendothelial markers [Figure 1]. All donors resulted strongly positive for stromal CD44-73-90 and negative for CD31 and CD45. CD34 resulted absent in hAMSCs and weakly positive in hASCs (6.6% ± 3.0%), as previously reported[41]. At Passage 3, hAMSCs reached a significantly higher confluence per cm^2 ($26.8 \times 10^3 \pm 2.9$ *vs.* $7.1 \times 10^3 \pm 0.2$, *P*-value of 0.0003).

In our experimental conditions, hASCs and hAMSCs released EVs in the range of $1.6 \times 10^3 \pm 0.4$ and $4.7 \times 10^3 \pm 1.9$ particles per cell (*P*-value of 0.01461) in 48 h, respectively. Overall, hAMSCs released 11.1-fold more EVs per surface unit (*P*-value of 0.00323) with respect to hASCs. NTA analysis confirmed the nanometer-scale range for both EV types [Figure 2A], the average size being 102 ± 8 nm and 96 ± 25 nm (mode ± SD) for hASC-EVs and hAMSC-EVs, respectively, with enrichment in small particles (75.1% ± 0.5% and 87.7% ± 4.4% below 200 nm). The dimensional range was confirmed by TEM [90 ± 37 and 90 ± 29 nm (mode ± SD) for hASC-EVs and hAMSC-EVs, respectively] [Figure 2B] and flow cytometry, after instrument calibration with fluorescent nanobeads (160, 200, 240, and 500 nm) [Figure 2C]. Both EV types resulted strongly positive for EV markers CD63 and CD81, while CD9 resulted barely detectable [Figure 2D]. In addition, MSC markers CD73 and CD90 were highly expressed, while CD44 appeared less abundant, although the whole peak shift suggests a homogeneous dim population.

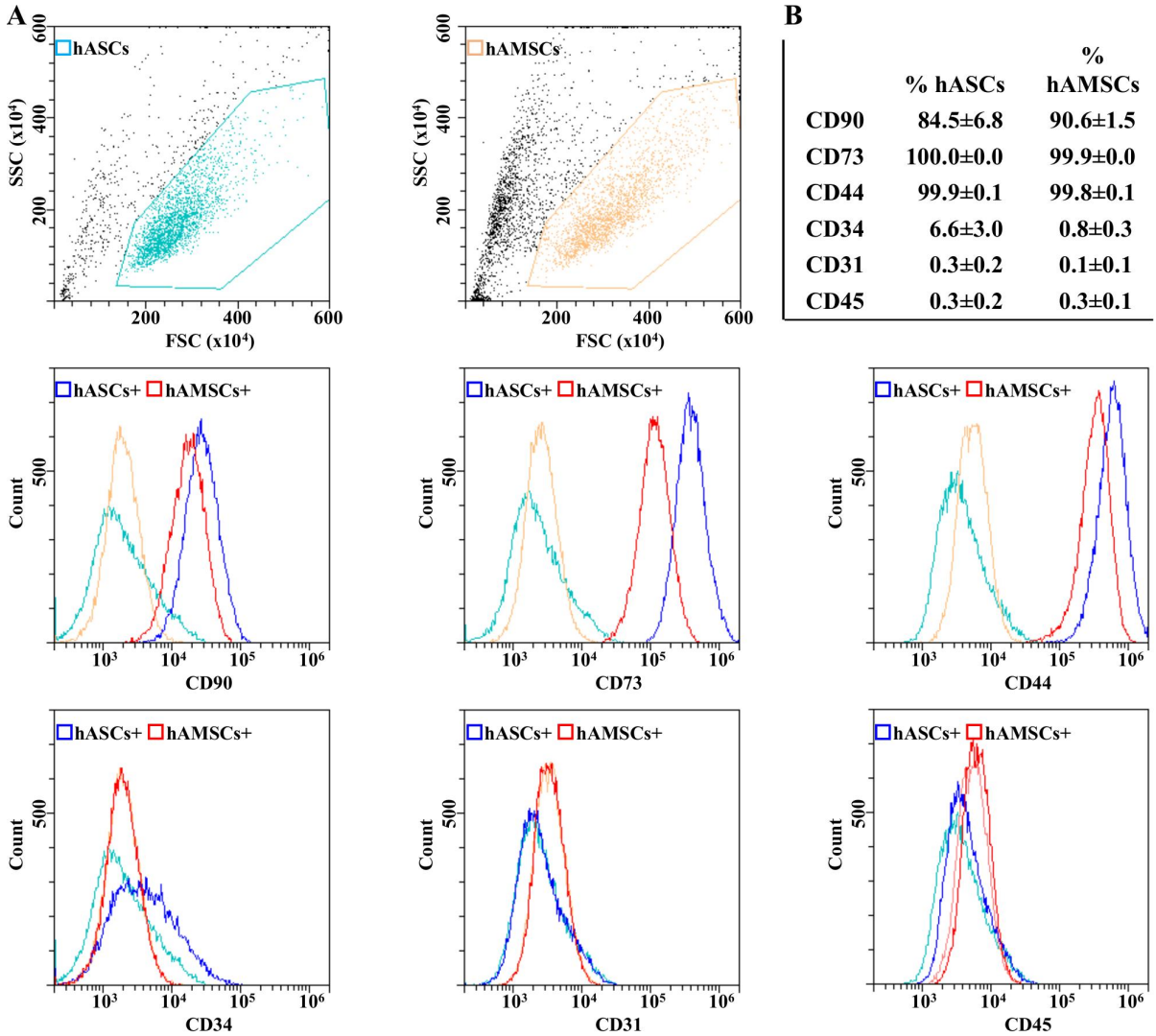

	% hASCs	% hAMSCs
CD90	84.5±6.8	90.6±1.5
CD73	100.0±0.0	99.9±0.0
CD44	99.9±0.1	99.8±0.1
CD34	6.6±3.0	0.8±0.3
CD31	0.3±0.2	0.1±0.1
CD45	0.3±0.2	0.3±0.1

Figure 1. hASCs and hAMSCs immunophenotype. (A) Flow cytometry analysis of hASC and hAMSCs for MSC (CD44/73/90) and hematoendothelial (CD31/34/45) markers. Representative plots are shown. (B) Percentage of positivity for analyzed markers obtained by averaging the three donors. Weak CD34 positivity is a landmark for hASCs identity.

EV-associated miRNAs

In total, 306 and 307 miRNAs were detected and highly shared in hASC-EVs and hAMSC-EVs, respectively (Supplementary Table 1), with miR-490-3p present only in hAMSC-EVs. Nevertheless, both PCA and hierarchical clustering were able to sharply cluster and group the EV types based on MSC origin [Figure 3A and B]. Accordingly, correlation analysis emphasized consistent homogeneity for both hASC-EV (R^2 of 0.96 ± 0.01) and hAMSC-EV (0.95 ± 0.02) donors, thus allowing to average EV miRNA C_{RT} values for each MSC type [Supplementary Table 2]. A reduced R^2 value (0.81) for averaged miRNAs emerged, confirming differential incorporation of the same miRNAs into EVs. Consistently, 47 candidates resulted upregulated (ratio > 2 between averaged values with P-value < 0.05 between populations) in hASC-EVs, with miR-30d-3p (ratio 998.30), miR-601 (179.44), and miR-95-3p being the ones with the highest fold change [Supplementary Table 2]. On the contrary, 71 molecules resulted downregulated (ratio < 0.5 with P-value < 0.05), and miR-372-3p (0.04), miR-30d-5p (0.01), and miR-146a-5p (0.0001) were the ones with the highest fold change [Supplementary Table 2].

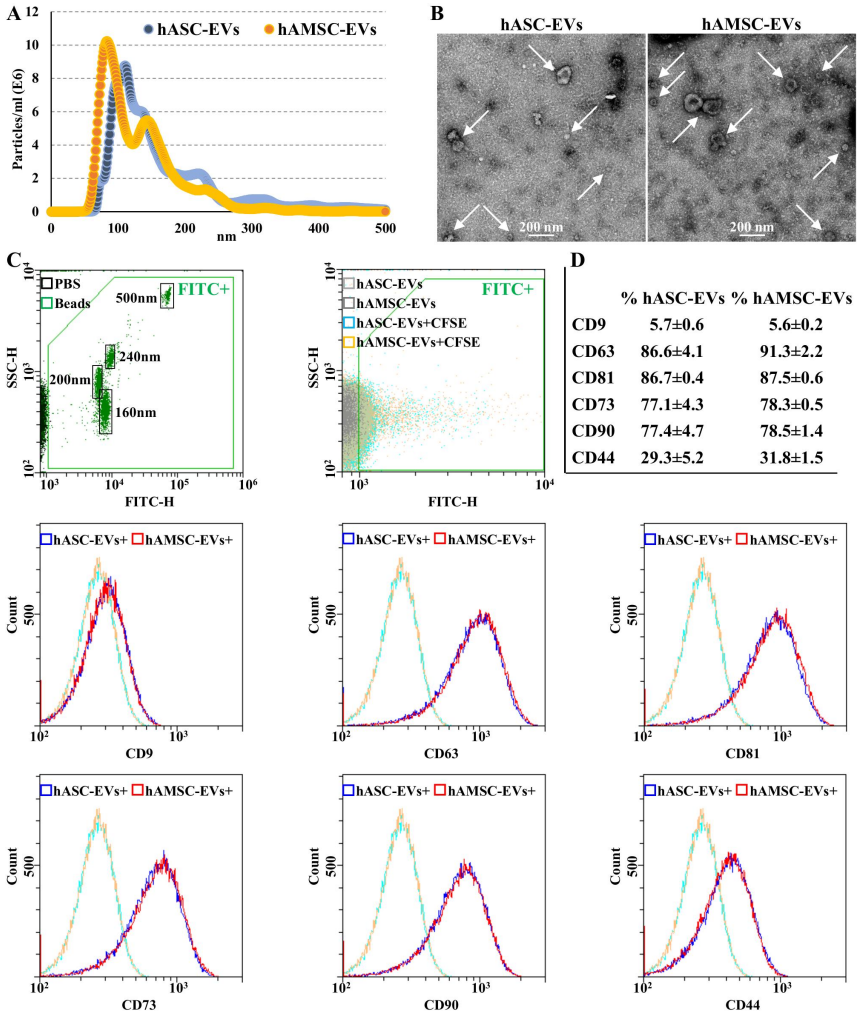

Figure 2. hASC-EVs and hAMSC-EVs characterization. (A) EV size distribution by NanoSight particle tracking analysis for both hASC-EVs (blue dots) and hAMSC-EVs (orange dots). Plots show merged data of the three donors for each MSC type. (B) Transmission electron micrographs of EVs showing particles with characteristic cup-shaped morphology. Representative donors are shown. (C) The resolution of the FITC-fluorescent reference nanobeads (160, 200, 240, and 500 nm) indicates the flow cytometer performance in light scattering at default settings. After flow cytometer calibration, CFSE-stained EVs can be identified and gated in the FITC channel (FITC+ gate) *vs.* unstained particles. After gating, with respect to Ab-unstained samples, both hASC-EVs and hAMSC-EVs showed the presence of EV-defining molecules CD63 and CD81, while CD9 staining gave a very weak signal. Both hASC-EVs and hAMSC-EVs were also positive for MSC markers CD73 and CD90. CD44 labeling allowed a complete peak shift of the population, although without a sharp peak separation. Representative cytograms are presented. (D) Percentage of positivity for analyzed markers obtained averaging the three donors. CFSE: Carboxyfluorescein succinimidyl ester; EVs: extracellular vesicles; FITC: fluorescein isothiocyanate; hASCs: adipose-derived mesenchymal stromal cells; hAMSCs: amniotic membrane-derived mesenchymal stromal cells.

To attribute a biological significance to detected or differentially expressed EV miRNAs, several parameters were taken into consideration: (1) even for the most abundant miRNA, in MSC-EVs no more than one copy per vesicle is present[42]; (2) a minimal ratio of 100 MSC-EVs per target cell is needed to allow transfer of abundant miRNAs[43]; and (3) in several cell types, including synoviocytes and chondrocytes, only a few thousand MSC-EVs can be incorporated in a day[32,44]. Therefore, only miRNAs laying in the first quartile of expression of both MSC-EV types were considered for further analysis. In total, 77 miRNAs defined each quartile [Table 1 and Supplementary Table 3 for those most abundantly (≥ 1% genetic weight) expressed], covering 97.90% and 98.19% of hASC-EVs and hAMSC-EVs genetic weight, respectively. Out of the selected molecules, 64 were shared, with 13 hASC-EVs and 13 hAMSC-EVs first quartile specific, collectively

Table 1. miRNAs differential expression and genetic weight in hASC-EVs *vs.* hAMSC-EVs first quartile of expression

miRBase ID	hASC-EVs % genetic weight	hAMSC-EVs % genetic weight	hASC-EVs *vs.* hAMSC-EVs ratio	*P*-value
miR-30d-3p	**0.11416**	0.00008	***998.30***	**0.00017**
miR-1260a	**0.16830**	0.00326	***35.56***	**0.00411**
let-7c-5p	**0.18163**	0.00523	***23.93***	**0.00017**
miR-195-5p	**0.12349**	0.00494	***17.20***	**0.00040**
miR-138-5p	**0.19066**	0.02287	***5.74***	**0.01210**
miR-27a-3p	**0.97429**	**0.12009**	***5.59***	**0.00752**
miR-29b-3p	**0.08998**	0.01442	***4.30***	**0.04382**
miR-125b-5p	**16.02689**	**2.67123**	***4.13***	**0.00278**
let-7a-5p	**0.18804**	0.03373	3.84	0.11638
miR-663b	**0.13204**	0.02513	3.62	0.09212
miR-30a-5p	**0.65026**	**0.14730**	***3.04***	**0.01300**
miR-224-5p	**0.54302**	**0.12461**	***3.00***	**0.02570**
miR-27b-3p	**0.35497**	**0.09320**	***2.62***	**0.04494**
miR-23a-3p	**0.10360**	0.02821	***2.53***	**0.03458**
miR-99b-5p	**1.57909**	**0.48102**	***2.26***	**0.02318**
miR-29c-3p	**0.43601**	**0.15005**	2.00	0.09116
miR-130a-3p	**0.63248**	**0.25032**	1.74	0.10744
miR-25-3p	**0.19648**	**0.08104**	1.67	0.06448
miR-218-5p	**0.76618**	**0.32756**	1.61	0.05748
miR-199a-3p	**0.89860**	**0.38569**	1.60	0.15468
miR-221-3p	**5.85265**	**2.67864**	1.50	0.15261
miR-143-3p	**0.11078**	0.05134	1.49	0.31951
miR-28-5p	**0.13638**	**0.06363**	1.48	0.45152
miR-26a-5p	**0.56739**	**0.29501**	1.32	0.56892
miR-31-3p	**0.33582**	**0.18152**	1.27	0.41762
miR-193b-3p	**4.27450**	**2.36882**	1.24	0.62762
miR-361-5p	**0.08915**	0.05027	1.22	0.20735
miR-21-5p	**6.27271**	**3.80748**	1.13	0.57381
miR-26b-5p	**0.14119**	**0.08680**	1.12	0.65301
miR-145-5p	**1.62348**	**1.02066**	1.10	0.82372
miR-148a-3p	**0.08532**	0.05467	1.07	0.89270
miR-34a-3p	**0.08280**	0.05310	1.07	0.60948
miR-100-5p	**3.60273**	**2.31365**	1.07	0.82076
miR-92a-3p	**1.59375**	**1.03563**	1.06	0.86197
miR-99a-5p	**3.56958**	**2.37924**	1.03	0.91251
miR-214-3p	**0.92173**	**0.62222**	1.02	0.94421
miR-106b-5p	**0.33427**	**0.22596**	1.02	0.91048
miR-365a-3p	**0.18038**	**0.12264**	1.01	0.95600
miR-16-5p	**0.44209**	**0.30443**	1.00	1.00000
miR-296-5p	**0.16445**	**0.11691**	0.97	0.92733
miR-22-3p	**0.15812**	**0.11945**	0.91	0.52628
miR-197-3p	**0.41632**	**0.31531**	0.91	0.84086

miR-34a-5p	**0.69052**	**0.55408**	0.86	0.39612
miR-152-3p	**0.52453**	**0.42933**	0.84	0.16680
miR-30b-5p	**2.34419**	**1.95455**	0.83	0.38278
miR-29a-3p	**0.98107**	**0.82198**	0.82	0.66389
miR-328-3p	**0.56739**	**0.48977**	0.80	0.65789
miR-10a-5p	**0.24527**	**0.21289**	0.79	0.67981
miR-222-3p	**5.20208**	**4.86634**	0.74	0.29980
miR-30c-5p	**3.05765**	**3.00737**	0.70	0.07172
miR-24-3p	**17.21693**	**17.70194**	0.67	0.01369
miR-130b-3p	**0.07797**	**0.08110**	0.66	0.10380
miR-132-3p	**0.48266**	**0.52456**	0.63	0.25039
miR-127-3p	**0.59698**	**0.66920**	0.61	0.11546
miR-382-5p	**0.59149**	**0.67245**	0.61	0.25318
miR-20a-5p	**1.44302**	**1.66075**	0.60	0.00791
miR-193a-5p	**0.16033**	**0.18636**	0.59	0.11502
miR-331-3p	**0.28109**	**0.32832**	0.59	0.26238
miR-28-3p	**0.10384**	**0.12264**	0.58	0.01535
miR-483-5	0.07480	**0.10421**	0.49	0.32196
miR-409-3p	**0.28109**	**0.41769**	0.46	0.24588
miR-532-5p	**0.08053**	**0.12435**	***0.45***	***0.00300***
miR-93-5p	0.06363	**0.10389**	***0.42***	***0.02717***
miR-654-5p	0.03629	**0.06309**	***0.40***	***0.03322***
miR-31-5p	**1.31260**	**2.31418**	0.39	0.28403
miR-30e-3p	**0.11181**	**0.20683**	***0.37***	***0.00791***
miR-495-3p	0.03546	**0.06875**	***0.36***	***0.03439***
miR-181a-5p	**0.10553**	**0.21397**	0.34	0.20687
miR-149-5p	**0.11104**	**0.22733**	***0.34***	***0.00459***
miR-30a-3p	**0.09666**	**0.22827**	***0.29***	***0.00031***
miR-376a-3p	**0.19739**	**0.46711**	***0.29***	***0.03306***
miR-320a-3p	**0.44209**	**1.09114**	***0.28***	***0.00161***
miR-886-5p	0.02914	**0.07749**	***0.26***	***0.00084***
miR-574-3p	**0.85407**	**2.30085**	***0.26***	***0.00221***
miR-19a-3p	0.02921	**0.08026**	***0.25***	***0.00024***
miR-17-5p	**0.44209**	**1.24934**	***0.24***	***0.00083***
miR-744-5p	0.02632	**0.07704**	***0.24***	***0.00654***
miR-106a-5p	**0.40214**	**1.21658**	***0.23***	***0.00324***
miR-210-3p	**0.15885**	**0.51293**	***0.21***	***0.00012***
miR-191-5p	**1.58274**	**5.37961**	***0.20***	***0.00029***
miR-186-5p	0.03394	**0.11907**	***0.20***	***0.00063***
miR-301a-3p	0.02302	**0.08117**	***0.20***	***0.00020***
miR-484	**0.41440**	**1.48538**	***0.19***	***0.00017***
miR-19b-3p	**1.19949**	**4.57520**	***0.18***	***0.00005***
miR-376c-3p	**0.14218**	**0.59385**	***0.16***	***0.00029***
miR-146b-5p	0.03059	**0.14615**	***0.14***	***0.00078***

miR-134-5p	0.01779	**0.11469**	***0.11***	***0.00135***
miR-342-3p	0.04701	**0.31824**	***0.10***	***0.00012***
miR-335-5p	**0.09402**	**0.67776**	***0.10***	***0.00480***
miR-146a-5p	0.00334	**16.38347**	***0.00***	***0.00026***

Bold indicates miRNAs in hASC-EVs or hAMSC-EVs first quartile of expression, while bold and italics indicates differentially abundant miRNAs (ratio > 2 or < 0.5 with *P*-value < 0.05).

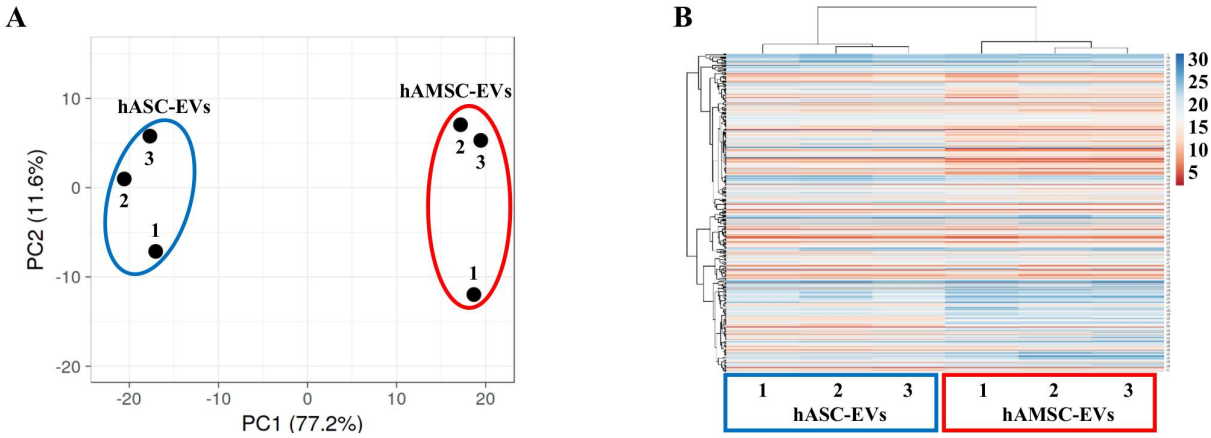

Figure 3. Comparison of hASC-EV- and hAMSC-EV-embedded miRNA abundance. (A) Principal component analysis of the normalized C_{RT} values of miRNAs. X and Y axes show Principal Components 1 and 2, which explain 77.2% and 11.6% of the total variance, respectively. (B) Heat map of hierarchical clustering analysis of the normalized C_{RT} values of detected miRNAs with sample clustering tree at the top. The color scale of normalized C_{RT} values reflects the absolute expression: red shades indicate high expression levels, while blue shades indicate low expression levels.

defining a group of 90 miRNAs. Within these candidates, 13 were significantly upregulated in hASC-EVs and 27 were downregulated, with miR-30d-3p being the most induced (ratio of 998.30) and miR-146a-5p the most reduced (0.0001). Sifting experimentally validated miRNA-mRNA interactions, first quartile hASC-EV miRNAs target 1575 univocal genes, while first quartile hAMSC-EVs 1543 transcripts. A high correlation emerged, with 1463 genes shared, 112 hASC-EV specific, and 80 hAMSC-EV specific. Overall, the 90 miRNAs resulted to target 1655 mRNAs [Supplementary Table 4 and 5]. In particular, 372 and 364 mRNAs are specifically targeted by 13 hASC-EV and 27 hAMSC-EV upregulated miRNAs, respectively [Supplementary Table 5]. These results suggest that single miRNA modulation of abundance between hASC-EVs and hAMSC-EVs, rather than different targets, frame the source-specific influence on target cells and tissues.

Target and effect prediction of EV miRNAs on OA tissues

To frame the effect of hASC-EV and hAMSC-EV miRNAs in the OA setting, validated targets of the 90 most abundant molecules were compared with synovia and/or cartilage-dependent regulators of OA progression[45] [Table 2]. This allowed obtaining the EV miRNA genetic weight for each targeted transcript. Regarding cytokines/chemokines, with the exception of anti-inflammatory IL4, all major OA-related inflammatory mediators, such as TNF, IFNG, IL1A/B, IL6 (and IL6-family related IL11), and IL18, are reported targets of EV miRNAs, with miR-125b-5p tipping the balance towards hASC-EVs for TNF and miR-191-5p towards hAMSC-EVs for IL1A. miR-146a-5p defined CXCL12, CCL5, CD40LG, and IL6 as hAMSC-EVs' preferred targets, while miR-125b-5p framed a superior hASC-EVs' regulation for EPO. Altogether, MSC-EVs appeared to interact with synovia-related inflammatory molecules. Regarding growth factors, TGFB1 emerged as the most heavily targeted transcript, with miR-146a-5p giving a higher weight to

Table 2. Soluble factors involved in OA pathological state and genetic weight of targeting EV miRNAs

	hASC-EVs total genetic weight (main regulator)	hAMSC-EVs total genetic weight (main regulator)	Function
Cytokines/chemokines			
IFNG	19.53% (miR-24-3p)	19.08% (miR-24-3p)	Pro-inflammatory
TNF	17.24% (miR-125b-5p)	4.30% (miR-125b-5p)	Pro-inflammatory
IL4	17.22% (miR-24-3p)	17.70% (miR-24-3p)	Anti-inflammatory
EPO	16.03% (miR-125b-3p)	2.67% (miR-125b-3p)	Upregulate Collagen, downregulate MMP-13
CXCL12	7.26% (miR-221-3p)	21.40% (miR-146a-5p)	Articular cartilage matrix degeneration
IL6	6.46% (miR-222-3p)	22.09% (miR-146a-5p)	Pro-inflammatory
IL1B	6.27% (miR-21-5p)	3.81% (miR-21-5p)	Pro-inflammatory
LIF	5.20% (miR-222-3p)	4.87% (miR-222-3p)	Cartilage erosion
IL11	3.06% (miR-30c-5p)	3.01% (miR-30c-5p)	Pro-inflammatory
IL1A	1.58% (miR-191-5p)	5.38% (miR-191-5p)	Pro-inflammatory
WNT1	1.54% (miR-34a-5p)	1.23% (miR-34a-5p)	Control Wnt signaling and aggravates OA pathology
CSF1	1.23% (miR-130a-3p)	0.76% (miR-152-3p)	Osteoclastogenesis enhancer, bone loss
CCL5	0.92% (miR-214-3p)	17.00% (miR-146a-5p)	Cartilage erosion
IL18	0.63% (miR-130a-3p)	0.25% (miR-130a-3p)	Pro-inflammatory
TNFSF11	0.33% (miR-106b-5p)	0.23% (miR-106b-5p)	Osteoclastogenesis enhancer, bone loss
CD40LG	0.00% (miR-146a-5p)	16.38% (miR-146a-5p)	Control the expression of inflammatory cytokines and MMP
Growth factors			
IGF2	19.95% (miR-125b-5p)	5.04% (miR-125b-5p)	Promote cartilage matrix levels
TGFB1	18.79% (miR-24-3p)	36.64% (miR-24-3p)	Cartilage homeostasis, high levels drive chondrocytes hypertrophy and synovial fibrosis
ANGPT2	18.70% (miR-125b-5p)	3.69% (miR-125b-5p)	Abnormal angiogenesis in OA
VEGFA	15.45% (miR-21-5p)	13.53% (miR-21-5p)	Promote OA process
TGFB2	7.97% (miR-21-5p)	4.89% (miR-21-5p)	Cartilage homeostasis, high levels released from joint tissue during OA development
CTGF	5.60% (miR-30c-5p)	4.47% (miR-30c-5p)	Promote osteophyte formation and ECM degradation
EGF	5.20% (miR-222-3p)	4.87% (miR-222-3p)	Promote chondrocyte catabolic activity
IGF1	3.78% (miR-29a-3p)	1.86% (miR-29a-3p)	Promote chondrocyte anabolic activity
BDNF	2.56% (miR-30a-5p)	2.13% (miR-132-3p)	Promote joint pain and inflammation
HGF	2.47% (miR-199a-3p)	1.40% (miR-199a-3p)	Cartilage homeostasis, promote osteophyte formation and osteoblast abnormal mineralization
FGF2	1.53% (miR-152-3p)	1.17% (miR-152-3p)	Promote catabolic and anti-anabolic effects in OA joints
BMP2	0.84% (miR-17-5p)	2.47% (miR-17-5p)	Promote cartilage regeneration
INHBB	0.69% (miR-34a-5p)	0.55% (miR-34a-5p)	TGFB superfamily, upregulatd in OA
KITLG	0.44% (miR-320a-3p)	1.09% (miR-320a-3p)	Promote synovial mast cell hyperplasia and inflammation
BMP6	0.16% (miR-22-3p)	0.12% (miR-22-3p)	Promote chondrocyte proliferation
TGFB3	0.09% (miR-29b-3p)	0.01% (miR-29b-3p)	Cartilage homeostasis, high levels released from joint tissue during OA development
PDGFC	0.09% (miR-29b-3p)	0.01% (miR-29b-3p)	Promote synovia MMP expression and angiogenesis
PDGFB	0.09% (miR-29b-3p)	0.01% (miR-29b-3p)	Promote subchondral bone angiogenesis
Proteases and other			
MMP2	31.92% (miR-125b-5p)	14.16% (miR-221-3p)	Metalloproteinase involved in ECM degradation
MMP13	20.69% (miR-125b-5p)	5.79% (miR-125b-3p)	Metalloproteinase involved in ECM degradation
MMP14	19.36% (miR-24-3p)	19.10% (miR-24-3p)	Metalloproteinase involved in ECM degradation
TIMP3	17.76% (miR-21-5p)	12.61% (miR-222-3p)	MMP inhibitor
APC	17.73% (miR-125b-5p)	4.24% (miR-125b-5p)	Promote MMP activity

MMP1	6.82% (miR-222-3p)	5.89% (miR-222-3p)	Metalloproteinase involved in ECM degradation
PLAT	6.27% (miR-21-5p)	3.81% (miR-21-5p)	ECM-degrading enzyme
PLAU	4.27% (miR-193b-3p)	2.37% (miR-193b-3p)	ECM-degrading enzyme
ADAM17	2.71% (miR-145-5p)	1.75% (miR-145-5p)	Metalloproteinase involved in ECM degradation
TIMP2	1.86% (miR-20a-5p)	2.96% (miR-20a-5p)	MMP inhibitor
ADAM12	1.60% (miR-29a-3p)	0.98% (miR-29a-3p)	Metalloproteinase involved in ECM degradation
ADAMTS9	0.98% (miR-29a-3p)	0.82% (miR-29a-3p)	Metalloproteinase involved in ECM degradation
MMP9	0.68% (miR-132-3p)	0.58% (miR-132-3p)	Metalloproteinase involved in ECM degradation
MMP15	0.53% (miR-29c-3p)	0.16% (miR-29c-3p)	Metalloproteinase involved in ECM degradation
ST14	0.35% (miR-27b-3p)	0.09% (miR-27b-3p)	Serine proteinase involved in cartilage destruction
TIMP1	0.11% (miR-181a-5p)	0.21% (miR-181a-5p)	MMP inhibitor
MMP3	0.06% (miR-93-5p)	0.10% (miR-93-5p)	Metalloproteinase involved in ECM degradation

hAMSC-EVs. On the contrary, TGFB2 regulation is strongest for hASC-EVs, due to miR-21-5p. In addition, hASC-EVs preferentially modulate protective IGF1/2, with the latter being a target of miR-125b-5p, which also framed the higher regulation of ANGPT2. Among other growth factors, VEGF, EGF, CTGF, HGF, and FGF2 are similarly modulated by the two EV types. Eventually, both MSC-EVs' miRNAs interact with several proteases secreted from both cartilage and synovia and involved in cartilage extracellular matrix degradation. The highest miRNA genetic weight emerged for MMP2/14/13/1 (in order of weight), with miR-125b-5p again tipping the balance towards hASC-EVs for MMP2/13. Of note, other proteases such as ADAM12/17, ADAMTS9, ST14, and plasminogen activators are also EV miRNA interactors. Interestingly, inhibitors of metalloproteases such as TIMPs laid among EV miRNA targets, although TIMP1/2 at lower levels with respect to TIMP3. miR-125b-5p framed hASC-EVs' preference for APC, involved in promoting MMP activity.

Investigating the general picture given by miRNAs reported to regulate the overall homeostasis of cartilage and synovia at different levels, at first, we focused on miRNAs that directly impact OA cartilage pathogenesis[46] [Table 3]. Eighteen protective and nine degenerative miRNAs were identified. hASC-EVs resulted enriched in miRNAs encompassing both categories (49% *vs.* 33% of EV genetic weight for protective, mainly due to miR-125b-5p, and 10% *vs.* 7% for destructive), with identical overall enrichment in OA-alleviating players, being the protective *vs.* destructive ratio 4.75 for both. Therefore, for cartilage, protective signals far exceeded damaging inputs. Notably, three miRNAs associated with overlapping roles in OA cartilage were present, and hAMSC-EV-specific miR-146a-5p had a strongly divergent expression. Regarding synovia, the definition of miRNA roles during OA progression is still in its infancy[47]. We identified two protecting and three damaging miRNAs [Table 3]. Albeit considering few players, no major differences between hASC-EVs and hAMSC-EVs could be detected, with again the preponderance for protecting players. Notably, as for cartilage, hAMSC-EV-specific miR-146a-5p was reported to have overlapping functions in synovia. To obtain further insight on synovia regulation, since many of the previously described cytokines/chemokines are mainly expressed by inflammatory cells, such as macrophages, we compared EV miRNAs with those reported to be involved in the macrophage M1 *vs.* M2 phenotype shift[48], considering M1 inflammatory macrophages as a synovial OA landmark. Seven miRNAs involved in M2 and six involved in M1 phenotype regulation were identified [Table 3]. M1 miRNAs resulted more abundant in hASC-EVs (3.3% *vs.* 1.7%), while M2 miRNAs were more present in hAMSC-EVs (39.9% *vs.* 23.3%). Therefore, although the M2 to M1 ratio always resulted in favor of anti-inflammatory macrophages, hAMSC-EVs had a greater impact on M2 polarization (ratio of 23 *vs.* 7), mainly due to miR-146-5p, responsible for the M1 to M2 switch.

Table 3. miRNAs involved in OA pathological state at cartilage, synovium, and macrophage levels

	hASC-EVs genetic weight	hAMSC-EVs genetic weight	Function
Cartilage protection			
miR-30a-3p	0.10%	0.23%	Cartilage homeostasis
miR-210-3p	0.16%	0.51%	Anti-apoptotic promotes chondrocyte proliferation and ECM deposition
miR-149-5p	0.11%	0.23%	Anti-inflammatory
miR-193b-3p	4.27%	2.37%	Regulates inflammation by repressing TNF-α expression
miR-320a	0.44%	1.09%	Chondrocyte viability
miR-148a-3p	0.09%	0.05%	Promotes hyaline cartilage production
miR-199a-3p	0.90%	0.39%	Anti-catabolic
miR-30a-5p	0.65%	0.15%	Cartilage homeostasis
miR-26b-5p	0.14%	0.09%	Cartilage homeostasis
miR-222-3p	5.20%	4.87%	Controls cartilage degradation
miR-26a-5p	0.57%	0.30%	Cartilage homeostasis
miR-27b-3p	0.35%	0.09%	Anti-catabolic
miR-24-3p	17.22%	17.70%	Regulates chondrocyte senescence
miR-92a-3p	1.59%	1.04%	Anti-catabolic and increases collagen deposition
miR-130a-3p	0.63%	0.25%	Anti-inflammatory
miR-17-5p	0.44%	1.25%	Induces autophagy
miR-19a-3p	0.03%	0.08%	Promotes chondrocyte viability and migration
mR-125b-5p	16.03%	2.67%	Prevents aggrecan loss
Cartilage destructive			
miR-16-5p	0.44%	0.30%	Cartilage degradation
miR-34a-5p	0.69%	0.55%	Apoptosis
miR-30b-5p	2.34%	1.95%	Pro-apoptotic, ECM degradation
miR-181a-5p	0.11%	0.21%	Pro-inflammatory, procatabolic, cell death
miR-21-5p	6.27%	3.81%	Negatively regulates chondrogenesis
miR-138-5p	0.19%	0.02%	Promotes cartilage degradation
miR-23a-3p	0.10%	0.03%	Inhibits ECM synthesis
miR-483-5p	0.07%	0.10%	Stimulates chondrocyte hypertrophy, ECM degradation
miR-34a-3p	0.08%	0.05%	Apoptosis
Cartilage overlapping			
miR-145-5p	1.62%	1.02%	Chondrocyte proliferation *vs.* cartilage degradation
miR-221-3p	5.95%	2.68%	Prevents ECM degradation *vs.* pro-inflammatory
miR-146a-5p	0.00%	16.38%	Chondrocyte proliferation, anti-apoptosis *vs.* activator of early OA
Synovia protection			
miR-26a-5p	0.57%	0.30%	Anti-inflammatory
miR-29a-3p	0.98%	0.82%	Protects against excessive synovial remodeling
Synovia destructive			
miR-34a-3p	0.08%	0.05%	Enhance synovial inflammation
miR-181a-5p	0.11%	0.21%	Enhance synovial inflammation
miR-210-3p	0.16%	0.51%	Pro-fibrotic
Synovia overlapping			
miR-146a-5p	0.00%	16.38%	Anti-inflammatory *vs.* promoting oxidative stress
Pro M1 macrophage			

miR-145-5p	1.62%	1.02%	M1 promoting
miR-27b-3p	0.35%	0.09%	M1 promoting, M2 suppressing
miR-130a-3p	0.63%	0.25%	M1 promoting, M2 suppressing
miR-19a-3p	0.03%	0.08%	M2 suppressing
miR-26a-5p	0.57%	0.30%	M2 suppressing
miR-195-5p	0.12%	0.00%	M2 suppressing
Pro M2 macrophage			
miR-24-3p	17.22%	17.70%	M2 promoting, M1 suppressing
miR-146a-5p	0.00%	16.38%	M2 promoting, M1 suppressing
miR-146b-5p	0.03%	0.15%	M2 promoting, M1 suppressing
miR-181a-5p	0.11%	0.21%	M2 promoting, M1 suppressing
miR-34a-5p	0.69%	0.55%	M2 promoting
miR-222-3p	5.20%	4.87%	M2 promoting
miR-301a-3p	0.02%	0.08%	M2 promoting

Identification of stable EV miRNA reference genes (RG)

To identify abundantly expressed and stable reference genes for future comparison analysis of novel miRNAs between hASC-EVs and hAMSC-EVs, four stability algorithms (Genorm, Normfinder, BestKeeper, and the comparative Delta Ct method) sifted the 64 miRNAs shared in both first quartiles (see Table 4 for the Top 10 and Supplementary Table 6 for the complete ranking). The most stable miRNAs were: (1) Genorm, miR-24-3p/127-3p (M-value of 0.00) and miR-34a-5p (0.27); (2) Normfinder, miR-34a-5p (SV of 0.25), miR-20a-5p (0.31), and miR-24-3p (0.34); (3) BestKeeper, miR-34a-5p (0.28), miR-30c-5p (0.28), and miR-99a-5p (0.28); and (4) Delta Ct, miR-34a-5p (0.87), miR-20a-5p (0.87), and miR-30c-5p (0.89). Notably, miR-27a-3p and miR-335-5p always resulted in the last two positions of the rankings. Eventually, the geometric mean (Geomean) of each putative RG weight across the four algorithms was calculated to identify a definitive hierarchy, considering the RG with the final lowest value as the most stable. miR-34a-5p clearly ranked best (Geomean of 1.73), while miR-335-5p laid in the last position (64).

DISCUSSION

In this report, EVs and embedded miRNAs from adipose- and amniotic membrane-derived MSCs, characterized with the same technical workflow and platform, were compared. In the frame of a shared overall molecular signature targeting several OA-related factors and processes, with few miRNAs tipping the balance, both hAMSCs and hASCs were able to release EVs with pro-M2 macrophage-polarizing and cartilage-protective cargo.

When selecting an MSC type to be envisioned as a therapeutic agent, several characteristics have to be taken into consideration. First, like the ease of accessibility and absence or low risk of morbidity. In this perspective, the collection of both adipose tissue and amniotic membrane, usually discarded in large amounts as waste material, has an advantage over bone marrow harvesting that requires a dedicated and often uncomfortable procedure to obtain reduced volumes of starting material. Second, amniotic membrane and adipose tissue have a high MSC content, in the range of 10^5-10^6 MSC per gram[8], and therefore largely more abundant than bone marrow[10]. Third, hAMSCs and hASCs showed superior immune regulation over bone marrow MSCs[49,50]. This has led to the creation of more and more hASCs/hASC products[51], and more recently hAMSCs and amniotic membrane-derived tissues[52] have gained attention in musculoskeletal regenerative medicine. Since the therapeutic potential of MSCs is ascribed to their secreted factors and EVs, a thorough characterization of these compartments is mandatory to envision the most effective source, especially for EVs that were recently proposed as standalone and cell-free medicinal agents for several pathologies[53], including OA[54]. In this frame, an often-underestimated issue is the EVs' secretory capacity.

Table 4. Top 10 hASC-EVs and hAMSC-EVs first quartile shared miRNAs' stability ranking

	Genorm M-value	Normfinder SV	BestKeeper SD	Delta CT SD	Geomean
miR-34a-5p	0.27	0.25	0.28	0.87	1.73
miR-24-3p	0.00	0.34	0.44	0.89	3.66
miR-20a-5p	0.36	0.31	0.50	0.87	4.52
miR-127-3p	0.00	0.34	0.44	0.89	4.53
miR-30c-5p	0.57	0.35	0.28	0.89	5.59
miR-99a-5p	0.46	0.37	0.28	0.90	6.09
miR-28-3p	0.41	0.35	0.44	0.90	7.65
miR-331-3p	0.44	0.45	0.33	0.94	7.90
miR-365a-3p	0.64	0.58	0.28	0.98	8.60
miR-106b-5p	0.58	0.59	0.28	1.00	10.03

This is crucial for both expanded MSCs and MSC-containing products, such as SVF or ASA, as well as for purified EVs. In the first case, a MSC type or source having a higher release of therapeutic and active EVs might have a stronger healing effect on target tissues. In addition, when purified EVs are produced as good manufacturing practice (GMP) products, a higher secretory ability will reduce the culture surface area per unit, the overall culturing time, and, by consequence, the cost of the production process for both the industry and national health system. In this study, we demonstrated that hAMSCs may release significantly more EVs per cell, which, in combination with a higher number of MSCs per gram of fresh tissues, suggests the secretion/collection of a greater number of hAMSC-EVs, both at the point-of-care and after *in vitro* expansion. We acknowledge that the different culture media used for hASCs and hAMSCs might have influenced cell physiology and secretory capacity, both the number of cells and the molecular content. Moreover, any *in vitro* condition is presumably far from the one those cells encounter in their therapeutic site (e.g., synovial fluid for OA treatment), possibly making the herein presented results not completely stackable with MSC behavior in cell-based therapeutic applications. Given these premises, we preferred cultivating cells in their specific and recognized media, as reported in the literature for *in vitro* expansion, considering media-related influence not a pitfall but a distinctive feature defining the fingerprint of currently used hASCs/hAMSCs and their secretomes/EVs. In this view, it will be crucial to understand whether therapeutic attributes of different MSCs and their EVs are due to the environmental conditions (site of administration, media, confluence, substrate, *etc.*), and whether by adjusting these conditions it is possible to optimize EVs for the target therapeutic application, as suggested in the last years for MSCs in general[55] and as demonstrated by our group for hASC-EV miRNAs after inflammatory priming[56]. Moreover, further characterization is needed to understand whether media-modulated MSC therapeutic attributes might be stable for some generations, making this option more attractive for cell therapies, or molecular changes are quickly transient as demonstrated for umbilical cord blood MSC intracellular miRNAs[57], suggesting media-based priming more indicated for cell-free therapies relying on secreted factors and EVs.

The second crucial issue defining cell expendability is the specific activity within a defined pathology. Many EV functions were ascribed to their nucleic acid content, especially miRNAs[58,59]. This was also demonstrated for MSC-EVs[60]. Therefore, given a similar number of EVs, the differential miRNA portfolio or its modulation may greatly impact the therapeutic message, taking also into account the biologically relevant miRNA concentration, biochemical functionality, and potential to elicit a timely response[43,61]. Moreover, although the amount of a regulatory molecule might allow a reliable prediction of its effects, since each miRNA may target several mRNA molecules, each present at a variable level of abundance and in different cellular districts possibly hindering its availability for interaction, it is not always possible to

directly predict the impact of single or few miRNAs on the target cell or tissue. Thus, all these factors were considered for the EV-miRNA analysis herein proposed, avoiding discussion of a few players with high expression but relying on those laying in the first quartile of expression and covering > 95% of the EV genetic message that, as a whole, resulted shared between hASC-EVs and hAMSC-EVs, since the vast majority of molecules are mutual. Nevertheless, the differential expression of a few players allowed sharply clustering the two tissue sources, regardless of donor variability. This is important since a conserved genetic message that goes beyond donor-dependent fluctuations is mandatory to predict constant efficacy on a specific disease. In the frame of OA, several abundant EV miRNAs targeted single factors[45] [Table 2] and fell within the general players[46] [Table 3] involved in disease pathogenesis. In the first category, many pro-inflammatory and synovia-specific cytokines[62] (TNF, IL6, IL1B, IL1A, IFNG, and IL18) are targeted. In particular, many of these key OA inflammatory mediators are secreted by synovia resident immune cells, including macrophages[45]. Intriguingly, together with the influence on macrophage secretion at a single factor level, where hASC-EVs had a greater impact on TNF due to miR-125b-5p and hAMSC-EVs on IL1A due to miR-191-5p and IL6 due to miR-146a-5p, miRNAs also had a profound influence on macrophage polarization. The macrophage anti-inflammatory phenotype was highly supported due to the presence of both pro-M2 and anti-M1 miRNAs, especially in hAMSC-EVs where the M2:M1 miRNA ratio was 23.5:7.1 in hASC-EVs. The discriminating factor was hAMSC-EVs enriched miR-146a-5p that in several studies reduced M1 and promoted M2 macrophage polarization[63-65]. Consistently, the only study comparing hASCs and hAMSCs activity on macrophages reported a higher capacity for M2 polarization in favor of hAMSCs[20]. Together with inflammatory factors, other OA-related and synovia specific cytokines are preferential hAMSC-EVs miRNA targeted. Among them, CXCL12 can induce chondrocyte death during the OA process[66] and its levels are increased in OA synovial fluid[67] and CCL5, one of the mediators most significantly elevated in OA synovial fluid[68], takes part in cartilage catabolism[69]. Conversely, EPO, which upregulates collagen expression while reducing MMP13, is more targeted by hASC-EVs due to miR-125b-5p. hAMSC-EVs' superior OA protective features also emerged for growth factors [Table 2]. In fact, in a shared scenario of OA driving factors targeting, such as VEGFA, CTGF, EGF, BDNF, and HGF, hAMSC-EVs more actively spotted TGFB1, which, at high and constant levels, as in OA patients, changes from a factor that blocks to a factor that facilitates chondrocyte hypertrophy, together with synovial fibrosis and osteophytes[70]. On the contrary, hASC-EVs more likely target IGF1 and especially IGF2, both having anabolic effects on cartilage, thus further reducing their bioavailability that is already suppressed in OA synovial fluid by the formation of high molecular weight complexes with their specific binding proteins[71]. Eventually, several molecules involved in cartilage ECM degradation, including MMPs and ADAM/ADAMTS[72], are highly targeted by EV miRNAs with respect to few inhibitors, especially TIMP3. In this case, hASC-EVs resulted preferential modulators, due to miR-125b-5p targeting of MMP2/13 and APC, involved in MMP2/13 activation[73]. A clear influence on the reduction of OA phenotype also emerged when comparing EV miRNAs with those involved in either disease or healing pathways, rather than sifting only single factors [Table 3]. In a scenario of general balance between hASC-EV and hAMSC-EV miRNAs, with identical overall protective *vs.* destructive ratio in favor or healing mechanisms, miR-125b-5p discriminated the two EV types, allowing hASC-EVs to have almost 50% of their miRNA genetic message involved in protective roles. The other EV-discriminating miRNA, hAMSC-related miR-146a-5p, was reported to have a dual function, being both an activator in early OA, enhancing cartilage destruction[46], and a repressor in late OA, by promoting chondrocyte proliferation and anti-apoptotic mechanisms through inhibition of NF-κB pathway[65]. And miR-146a-5p was also described as having a dual role in the synovium[47], being both anti-inflammatory and an inducer of oxidative stress. Nevertheless, miRNAs' role in synovia is still underestimated, and available data do not allow a deep evaluation of EVs' impact on the tissue. An example is miR-125b-5p, the expression of which increases with OA severity and inhibits synovial cell proliferation by promoting apoptosis, being therefore considered a pathological miRNA[74]. Nevertheless, miR-125b-5p upregulation might also be an attempt to attenuate synovial hyperplasia and

fibrosis in an effort to maintain normal synovial function rather than contributing to pathologic OA disease progression. Therefore, at present, a clear role for miR-125b-5p is unclear, and we could not include this miRNA in the analyzed categories.

We are aware that one of the main limitations of this study, together with the restricted description of miRNA function for several tissues, was the limited number of tested miRNAs. We preferred to focus on well-described molecules, recognizing that several new miRNAs are discovered on an almost daily basis. For this reason, a reliable normalization strategy for future evaluations is mandatory. The most sensitive quantification approach is the miRNA global mean expression, relying on obtaining a large portfolio of the miRNome[75]. Accordingly, we used this method for whole dataset comparison. Nevertheless, preparation of a large volume of EVs and an expensive high throughput search would be needed each time different samples are compared, making the process unsustainable for both research applications, studying single or few miRNAs, and clinical trials with GMP batches. This is in fact another major issue that has also been debated recently for EVs from umbilical cord-derived MSCs, in order to facilitate translational research[76]. In this context, to the best of our knowledge, studies comparing hASCs and hAMSCs do not suggest miRNA reference genes in general, or for EVs in particular. Therefore, we wanted to obtain reference genes behaving similarly to the global mean approach, and bioinformatics was applied to normalized data in place of raw values. With these premises, miR-34a-5p clearly resulted the best candidate. Interestingly, miR-16-5p, which resulted the most stable according to averaged C_{RT} values (hASC-EVs *vs*. hAMSC-EVs ratio of 1), ranked 26th, suggesting that overall stability might mask fluctuations at the donor level.

In conclusion, both EV types possessed chondro-protective and pro-M2 macrophage features due to several embedded miRNAs. These results provide, at least for the EV miRNA role, the molecular basis for the significant improvement driven by hASC- and hAMSC-based products in terms of inflammation reduction and joint function observed in pivotal clinical studies. Molecular data suggest stronger commitment in anti-inflammatory macrophage modulation for hAMSC-EVs and a less defined picture for the definition of the best EV type in cartilage protection, where harmful growth factors are the preferential hAMSC-EV target, whereas ECM was more protected by hASC-EVs' inhibitory activity on proteases and the presence of miR-125b-5p. The observed *in vitro* increased chondro-protection and M1:M2 synovial macrophage ratio reduction for hAMSCs with respect to hASCs[20] might be due to the highest EV release of hAMSCs that can overcome the similar chondro-protective ability. Future clinical studies to address the issue regarding EVs dose will be necessary, especially in the frame of GMP clinical products. Regarding MSC-enriched, tissue-based, one-step procedures, the feasibility of tissue harvesting, the ease of bedside treatment, and the allogeneic *vs*. autologous issue might drive adipose or amniotic membrane tissue selection, both relying on active OA healing and counteracting MSC populations.

DECLARATIONS

Authors' contributions

Conception and design, collection and assembly of data, data analysis and interpretation, statistical analysis and manuscript writing: Ragni E, Perucca Orfei C, Papait A
Financial support and final approval of manuscript: de Girolamo L

Availability of data and materials

Not applicable.

Financial support and sponsorship

This work was supported by the Italian Ministry of Health, "Ricerca Corrente". Funding body had no involvement in the experiment design, collection, analysis and interpretation of data, and writing of the

manuscript. Authors acknowledge Regenerative Medicine Research Center (CROME) of Università Cattolica del Sacro Cuore. This work contributes to COST Action CA17116 International Network for Translating Research on Perinatal Derivatives into Therapeutic Approaches (SPRINT), supported by COST (European Cooperation in Science and Technology).

Conflicts of interest

All authors declared that there are no conflicts of interest.

Ethical approval and consent to participate

Not applicable.

Consent for publication

Not applicable.

Copyright

REFERENCES

1. Hunter DJ, March L, Chew M. Osteoarthritis in 2020 and beyond: a Lancet commission. *Lancet* 2020;396:1711-2. DOI PubMed
2. Hunter DJ, Bierma-zeinstra S. Osteoarthritis. *Lancet* 2019;393:1745-59. DOI PubMed
3. Rannou F, Pelletier JP, Martel-Pelletier J. Efficacy and safety of topical NSAIDs in the management of osteoarthritis: evidence from real-life setting trials and surveys. *Semin Arthritis Rheum* 2016;45:S18-21. DOI PubMed
4. Lopa S, Colombini A, Moretti M, de Girolamo L. Injective mesenchymal stem cell-based treatments for knee osteoarthritis: from mechanisms of action to current clinical evidences. *Knee Surg Sports Traumatol Arthrosc* 2019;27:2003-20. DOI PubMed PMC
5. Caplan AI. Mesenchymal stem cells: time to change the name! *Stem Cells Transl Med* 2017;6:1445-51. DOI PubMed PMC
6. Ferrero R, Rainer P, Deplancke B. Toward a consensus view of mammalian adipocyte stem and progenitor cell heterogeneity. *Trends Cell Biol* 2020;30:937-50. DOI PubMed
7. Silini AR, Di Pietro R, Lang-Olip I, et al. Perinatal derivatives: where do we stand? *Front Bioeng Biotechnol* 2020;8:610544. DOI PubMed PMC
8. Wu M, Zhang R, Zou Q, et al. Comparison of the biological characteristics of mesenchymal stem cells derived from the human placenta and umbilical cord. *Sci Rep* 2018;8:5014. DOI PubMed PMC
9. Bravenboer N, Bredella MA, Chauveau C, et al. Standardised nomenclature, abbreviations, and units for the study of bone marrow adiposity: report of the nomenclature working group of the international bone marrow adiposity society. *Front Endocrinol (Lausanne)* 2019;10:923. DOI PubMed PMC
10. Galotto M, Berisso G, Delfino L, et al. Stromal damage as consequence of high-dose chemo/radiotherapy in bone marrow transplant recipients. *Exp Hematol* 1999;27:1460-6. DOI PubMed
11. Maleitzke T, Elazaly H, Festbaum C, et al. Mesenchymal stromal cell-based therapy-an alternative to arthroplasty for the treatment of osteoarthritis? *J Clin Med* 2020;9:2062. DOI PubMed PMC
12. Cho H, Kim H, Kim YG, Kim K. Recent clinical trials in adipose-derived stem cell mediated osteoarthritis treatment. *Biotechnol Bioproc E* 2019;24:839-53. DOI
13. Moschini M, Zamboni S, Mattei A. Re: Kristian D. Stensland, Harras Zaid, Mark Broadwin, et al. Comparative effectiveness of treatment strategies for squamous cell carcinoma of the bladder. Eur Urol Oncol. In press. https://doi.org/10.1016/j.euo.2018.11.003. *Eur Urol Oncol* 2019;2:230. DOI PubMed
14. Vines JB, Aliprantis AO, Gomoll AH, Farr J. Cryopreserved amniotic suspension for the treatment of knee osteoarthritis. *J Knee Surg* 2016;29:443-50. DOI PubMed
15. Farr J, Gomoll AH, Yanke AB, Strauss EJ, Mowry KC; ASA Study Group. A randomized controlled single-blind study demonstrating superiority of amniotic suspension allograft injection over hyaluronic acid and saline control for modification of knee osteoarthritis symptoms. *J Knee Surg* 2019;32:1143-54. DOI PubMed
16. Gomoll AH, Farr J, Cole BJ, et al. Safety and efficacy of an amniotic suspension allograft injection over 12 months in a single-blinded, randomized controlled trial for symptomatic osteoarthritis of the knee. *Arthroscopy* 2021;37:2246-57. DOI PubMed
17. Shariatzadeh M, Song J, Wilson SL. Correction to: the efficacy of different sources of mesenchymal stem cells for the treatment of knee osteoarthritis. *Cell Tissue Res* 2019;378:559. DOI PubMed
18. Song Y, Zhang J, Xu H, et al. Mesenchymal stem cells in knee osteoarthritis treatment: A systematic review and meta-analysis. *J Orthop Translat* 2020;24:121-30. DOI PubMed
19. Topoluk N, Hawkins R, Tokish J, Mercuri J. Amniotic mesenchymal stromal cells exhibit preferential osteogenic and chondrogenic differentiation and enhanced matrix production compared with adipose mesenchymal stromal cells. *Am J Sports Med* 2017;45:2637-46. DOI PubMed PMC

20. Topoluk N, Steckbeck K, Siatkowski S, Burnikel B, Tokish J, Mercuri J. Amniotic mesenchymal stem cells mitigate osteoarthritis progression in a synovial macrophage-mediated in vitro explant coculture model. *J Tissue Eng Regen Med* 2018;12:1097-110. DOI PubMed PMC
21. Ragni E, Papait A, Perucca Orfei C, et al. Amniotic membrane-mesenchymal stromal cells secreted factors and extracellular vesicle-miRNAs: Anti-inflammatory and regenerative features for musculoskeletal tissues. *Stem Cells Transl Med* 2021;10:1044-62. DOI PubMed PMC
22. Tofiño-Vian M, Guillén MI, Pérez Del Caz MD, Silvestre A, Alcaraz MJ. Microvesicles from human adipose tissue-derived mesenchymal stem cells as a new protective strategy in osteoarthritic chondrocytes. *Cell Physiol Biochem* 2018;47:11-25. DOI PubMed
23. Tofiño-Vian M, Guillén MI, Pérez Del Caz MD, Castejón MA, Alcaraz MJ. Extracellular vesicles from adipose-derived mesenchymal stem cells downregulate senescence features in osteoarthritic osteoblasts. *Oxid Med Cell Longev* 2017;2017:7197598. DOI PubMed PMC
24. Boulestreau J, Maumus M, Rozier P, Jorgensen C, Noel D. Senescence did not alter the chondroprotective effect of extracellular vesicles from adipose mesenchymal stem cells in osteoarthritis. *Osteoarthritis and Cartilage* 2021;29:S68. DOI
25. Ragni E, Colombini A, Viganò M, et al. Cartilage protective and immunomodulatory features of osteoarthritis synovial fluid-treated adipose-derived mesenchymal stem cells secreted factors and extracellular vesicles-embedded miRNAs. *Cells* 2021;10:1072. DOI PubMed PMC
26. Heo JS, Choi Y, Kim HO. Adipose-derived mesenchymal stem cells promote M2 macrophage phenotype through exosomes. *Stem Cells Int* 2019;2019:7921760. DOI PubMed PMC
27. Domenis R, Cifù A, Quaglia S, et al. Pro inflammatory stimuli enhance the immunosuppressive functions of adipose mesenchymal stem cells-derived exosomes. *Sci Rep* 2018;8:13325. DOI PubMed PMC
28. Zhang S, Chuah SJ, Lai RC, Hui JHP, Lim SK, Toh WS. MSC exosomes mediate cartilage repair by enhancing proliferation, attenuating apoptosis and modulating immune reactivity. *Biomaterials* 2018;156:16-27. DOI PubMed
29. Zhang J, Rong Y, Luo C, Cui W. Bone marrow mesenchymal stem cell-derived exosomes prevent osteoarthritis by regulating synovial macrophage polarization. *Aging (Albany NY)* 2020;12:25138-52. DOI PubMed PMC
30. Jiang S, Tian G, Yang Z, et al. Enhancement of acellular cartilage matrix scaffold by Wharton's jelly mesenchymal stem cell-derived exosomes to promote osteochondral regeneration. *Bioact Mater* 2021;6:2711-28. DOI PubMed PMC
31. Qiu G, Zheng G, Ge M, et al. Mesenchymal stem cell-derived extracellular vesicles affect disease outcomes via transfer of microRNAs. *Stem Cell Res Ther* 2018;9:320. DOI PubMed PMC
32. Ragni E, Perucca Orfei C, De Luca P, et al. Interaction with hyaluronan matrix and miRNA cargo as contributors for in vitro potential of mesenchymal stem cell-derived extracellular vesicles in a model of human osteoarthritic synoviocytes. *Stem Cell Res Ther* 2019;10:109. DOI PubMed PMC
33. D'haene B, Mestdagh P, Hellemans J, Vandesompele J. miRNA expression profiling: from reference genes to global mean normalization. *Methods Mol Biol* 2012;822:261-72. DOI PubMed
34. Vandesompele J, De Preter K, Pattyn F, et al. Accurate normalization of real-time quantitative RT-PCR data by geometric averaging of multiple internal control genes. *Genome Biol* 2002;3:RESEARCH0034. DOI PubMed PMC
35. Andersen CL, Jensen JL, Ørntoft TF. Normalization of real-time quantitative reverse transcription-PCR data: a model-based variance estimation approach to identify genes suited for normalization, applied to bladder and colon cancer data sets. *Cancer Res* 2004;64:5245-50. DOI PubMed
36. Pfaffl MW, Tichopad A, Prgomet C, Neuvians TP. Determination of stable housekeeping genes, differentially regulated target genes and sample integrity: BestKeeper - excel-based tool using pair-wise correlations. *Biotechnology Letters* 2004;26:509-15. DOI PubMed
37. Silver N, Best S, Jiang J, Thein SL. Selection of housekeeping genes for gene expression studies in human reticulocytes using real-time PCR. *BMC Mol Biol* 2006;7:33. DOI PubMed PMC
38. Xie F, Xiao P, Chen D, Xu L, Zhang B. miRDeepFinder: a miRNA analysis tool for deep sequencing of plant small RNAs. *Plant Mol Biol* 2012. DOI PubMed
39. Metsalu T, Vilo J. ClustVis: a web tool for visualizing clustering of multivariate data using Principal Component Analysis and heatmap. *Nucleic Acids Res* 2015;43:W566-70. DOI PubMed PMC
40. Chou CH, Shrestha S, Yang CD, et al. miRTarBase update 2018: a resource for experimentally validated microRNA-target interactions. *Nucleic Acids Res* 2018;46:D296-302. DOI PubMed PMC
41. Mitchell JB, McIntosh K, Zvonic S, et al. Immunophenotype of human adipose-derived cells: temporal changes in stromal-associated and stem cell-associated markers. *Stem Cells* 2006;24:376-85. DOI PubMed
42. Toh WS, Lai RC, Hui JHP, Lim SK. MSC exosome as a cell-free MSC therapy for cartilage regeneration: Implications for osteoarthritis treatment. *Semin Cell Dev Biol* 2017;67:56-64. DOI PubMed
43. Chevillet JR, Kang Q, Ruf IK, et al. Quantitative and stoichiometric analysis of the microRNA content of exosomes. *Proc Natl Acad Sci U S A* 2014;111:14888-93. DOI PubMed PMC
44. Ragni E, Palombella S, Lopa S, et al. Innovative visualization and quantification of extracellular vesicles interaction with and incorporation in target cells in 3D microenvironments. *Cells* 2020;9:1180. DOI PubMed PMC
45. Chou CH, Jain V, Gibson J, et al. Synovial cell cross-talk with cartilage plays a major role in the pathogenesis of osteoarthritis. *Sci Rep* 2020;10:10868. DOI PubMed PMC
46. Endisha H, Rockel J, Jurisica I, Kapoor M. The complex landscape of microRNAs in articular cartilage: biology, pathology, and

therapeutic targets. *JCI Insight* 2018;3:121630. DOI PubMed PMC
47. Tavallaee G, Rockel JS, Lively S, Kapoor M. MicroRNAs in synovial pathology associated with osteoarthritis. *Front Med (Lausanne)* 2020;7:376. DOI PubMed PMC
48. Xu SJ, Hu HT, Li HL, Chang S. The role of miRNAs in immune cell development, immune cell activation, and tumor immunity: with a focus on macrophages and natural killer cells. *Cells* 2019;8:1140. DOI PubMed PMC
49. Rossi D, Pianta S, Magatti M, Sedlmayr P, Parolini O. Characterization of the conditioned medium from amniotic membrane cells: prostaglandins as key effectors of its immunomodulatory activity. *PLoS One* 2012;7:e46956. DOI PubMed PMC
50. Zhu C, Wu W, Qu X. Mesenchymal stem cells in osteoarthritis therapy: a review. *Am J Transl Res* 2021;13:448-61. PubMed PMC
51. Shukla L, Yuan Y, Shayan R, Greening DW, Karnezis T. Fat therapeutics: the clinical capacity of adipose-derived stem cells and exosomes for human disease and tissue regeneration. *Front Pharmacol* 2020;11:158. DOI PubMed PMC
52. Díaz-Prado S, Muiños-López E, Hermida-Gómez T, et al. Human amniotic membrane as an alternative source of stem cells for regenerative medicine. *Differentiation* 2011;81:162-71. DOI PubMed
53. Phinney DG, Pittenger MF. Concise review: MSC-derived exosomes for cell-free therapy. *Stem Cells* 2017;35:851-8. DOI PubMed
54. Mianehsaz E, Mirzaei HR, Mahjoubin-Tehran M, et al. Mesenchymal stem cell-derived exosomes: a new therapeutic approach to osteoarthritis? *Stem Cell Res Ther* 2019;10:340. DOI PubMed PMC
55. Noronha NC, Mizukami A, Caliári-Oliveira C, et al. Priming approaches to improve the efficacy of mesenchymal stromal cell-based therapies. *Stem Cell Res Ther* 2019;10:131. DOI PubMed PMC
56. Ragni E, Perucca Orfei C, De Luca P, et al. Inflammatory priming enhances mesenchymal stromal cell secretome potential as a clinical product for regenerative medicine approaches through secreted factors and EV-miRNAs: the example of joint disease. *Stem Cell Res Ther* 2020;11:165. DOI PubMed PMC
57. Ragni E, Parazzi V, Crosti M, Moro M, Giordano R, Lazzari L. Diet composition transiently modulates proliferative and potency features of human cord blood-derived mesenchymal stem cells. *Int J Biochem Cell Biol* 2014;55:269-78. DOI PubMed
58. O'Brien K, Breyne K, Ughetto S, Laurent LC, Breakefield XO. RNA delivery by extracellular vesicles in mammalian cells and its applications. *Nat Rev Mol Cell Biol* 2020;21:585-606. DOI PubMed PMC
59. Mori MA, Ludwig RG, Garcia-Martin R, Brandão BB, Kahn CR. Extracellular miRNAs: from biomarkers to mediators of physiology and disease. *Cell Metab* 2019;30:656-73. DOI PubMed PMC
60. Ferguson SW, Wang J, Lee CJ, et al. The microRNA regulatory landscape of MSC-derived exosomes: a systems view. *Sci Rep* 2018;8:1419. DOI PubMed PMC
61. Toh WS, Lai RC, Zhang B, Lim SK. MSC exosome works through a protein-based mechanism of action. *Biochem Soc Trans* 2018;46:843-53. DOI PubMed PMC
62. Chow YY, Chin KY. The role of inflammation in the pathogenesis of osteoarthritis. *Mediators Inflamm* 2020;2020:8293921. DOI PubMed PMC
63. Zhang Y, Zhang M, Zhong M, Suo Q, Lv K. Expression profiles of miRNAs in polarized macrophages. *Int J Mol Med* 2013;31:797-802. DOI PubMed
64. Vergadi E, Vaporidi K, Theodorakis EE, et al. Akt2 deficiency protects from acute lung injury via alternative macrophage activation and miR-146a induction in mice. *J Immunol* 2014;192:394-406. DOI PubMed
65. Taganov KD, Boldin MP, Chang KJ, Baltimore D. NF-kappaB-dependent induction of microRNA miR-146, an inhibitor targeted to signaling proteins of innate immune responses. *Proc Natl Acad Sci U S A* 2006;103:12481-6. DOI PubMed PMC
66. Wei L, Sun X, Kanbe K, Wang Z, Sun C, et al. Chondrocyte death induced by pathological concentration of chemokine stromal cell-derived factor-1. *J Rheumatol* 2006;33:1818-26. PubMed
67. Xu Q, Sun XC, Shang XP, Jiang HS. Association of CXCL12 levels in synovial fluid with the radiographic severity of knee osteoarthritis. *J Investig Med* 2012;60:898-901. DOI PubMed
68. Monibi F, Roller BL, Stoker A, Garner B, Bal S, Cook JL. Identification of synovial fluid biomarkers for knee osteoarthritis and correlation with radiographic assessment. *J Knee Surg* 2016;29:242-7. DOI PubMed
69. Borzì RM, Mazzetti I, Marcu KB, Facchini A. Chemokines in cartilage degradation. *Clin Orthop Relat Res* 2004:S53-61. DOI PubMed
70. der Kraan PM. Differential role of transforming growth factor-beta in an osteoarthritic or a healthy joint. *J Bone Metab* 2018;25:65-72. DOI PubMed PMC
71. Bączyk J, Gogiel T, Wolańska M, et al. IGFs and IGF-binding proteins in the synovial fluid of patients with rheumatoid arthritis and osteoarthritis. *Int J Pept Res Ther* 2020;26:271-80. DOI
72. Wilkinson DJ, Arques MDC, Huesa C, Rowan AD. Serine proteinases in the turnover of the cartilage extracellular matrix in the joint: implications for therapeutics. *Br J Pharmacol* 2019;176:38-51. DOI PubMed PMC
73. Jackson MT, Moradi B, Smith MM, Jackson CJ, Little CB. Activation of matrix metalloproteinases 2, 9, and 13 by activated protein C in human osteoarthritic cartilage chondrocytes. *Arthritis Rheumatol* 2014;66:1525-36. DOI PubMed
74. Ge FX, Li H, Yin X. Upregulation of microRNA-125b-5p is involved in the pathogenesis of osteoarthritis by downregulating SYVN1. *Oncol Rep* 2017;37:2490-6. DOI PubMed
75. Mestdagh P, Van Vlierberghe P, De Weer A, et al. A novel and universal method for microRNA RT-qPCR data normalization. *Genome Biol* 2009;10:R64. DOI PubMed PMC
76. Rohde E, Pachler K, Gimona M. Manufacturing and characterization of extracellular vesicles from umbilical cord-derived mesenchymal stromal cells for clinical testing. *Cytotherapy* 2019;21:581-92. DOI PubMed

Zhao *et al. Extracell Vesicles Circ Nucleic Acids* 2021;2:222-3
DOI: 10.20517/evcna.2021.15

Extracellular Vesicles and Circulating Nucleic Acids

Erratum

Open Access

Erratum: Isolation and analysis methods of extracellular vesicles (EVs)

Zheng Zhao[1,2], Harshani Wijerathne[3], Andrew K. Godwin[6], Steven A. Soper[1,2,4,5,6,7]

[1]Bioengineering Program, University of Kansas, Lawrence, KS 66045, USA.
[2]Center of BioModular Multiscale Systems for Precision Medicine, Lawrence, KS 66045, USA.
[3]Department of Mechanical Engineering, Temple University, Philadelphia, PA 19122, USA.
[4]Department of Chemistry, University of Kansas, Lawrence, KS 66045, USA.
[5]Department of Mechanical Engineering, University of Kansas, Lawrence, KS 66045, USA.
[6]KU Cancer Center, University of Kansas Medical Center, Kansas City, KS 66160, USA.
[7]Ulsan National Institute of Science & Technology, Ulju-gun, Ulsan 44919, South Korea.

Correspondence to: Prof. Steven A. Soper, Department of Chemistry, Department of Mechanical Engineering, The University of Kansas, 1567 Irving Hill Road, Lawrence, KS 66045, USA. E-mail: ssoper@ku.edu

How to cite this article: Zhao Z, Wijerathne H, Godwin AK, Soper SA. Erratum: Isolation and analysis methods of extracellular vesicles (EVs). *Extracell Vesicles Circ Nucleic Acids* 2021;2:222-3. https://dx.doi.org/10.20517/evcna.2021.15

Received: 25 Aug 2021 **Accepted:** 7 Sep 2021 **Available online:** 15 Sep 2021

Academic Editor: Yoke Peng Loh **Copy Editor:** Xi-Jun Chen **Production Editor:** Xi-Jun Chen

This is an Erratum of the publsihed paper: Isolation and analysis methods of extracellular vesicles (EVs).

The authors wish to make the following corrections to this paper[1].

(1) In Figure 7A, a reference is missing, and the authors want to update it as follow:

(2) The addition of a reference to the citation list:

203. He N, Thippabhotla S, Zhong C, et al. Nano Pom-poms prepared highly specific extracellular vesicles expand the detectable cancer biomarkers. *BioRxiv* 2021.

The authors apologize for any inconvenience caused and state that the scientific conclusions are unaffected. The original article has been updated.

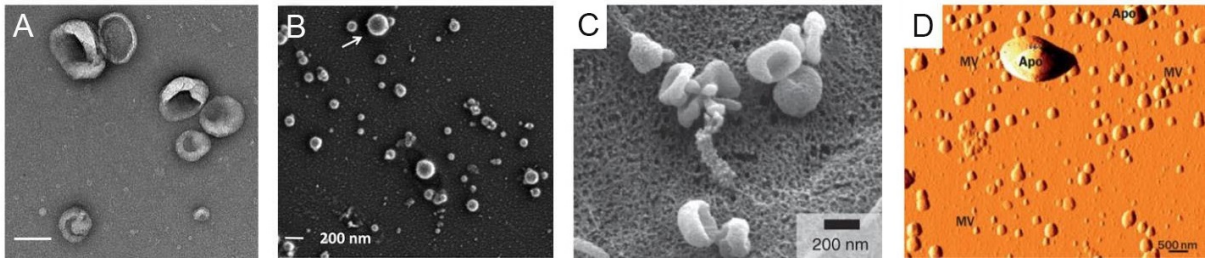

Figure 7. (A) Transmission electron microscopy image of EVs (scale bar = 100 nm)[203]. (B) Scanning electron microscope image of EVs showing the EVs' circular shape (reproduced from[151]). (C) Scanning electron microscope image of EVs, which shows cup-shaped EVs (reproduced from[150]). (D) Atomic force microscope image for EVs (reproduced from[156]). (Figure 7A is produced from He *et al.*'s work with permission).

REFERENCES

1. Zhao Z, Wijerathne H, Godwin AK, Soper SA. Isolation and analysis methods of extracellular vesicles (EVs). *Extracell Vesicles Circ Nucleic Acids* 2021;2:80-103. DOI

Tamura *et al. Extracell Vesicles Circ Nucleic Acids* 2021;2:224-7
DOI: 10.20517/evcna.2021.14

Extracellular Vesicles and Circulating Nucleic Acids

Commentary

Open Access

Check for updates

Extracellular vesicles as the "magic bullet" for fighting threats to humanity

Takaaki Tamura[1,2], Yusuke Yoshioka[1], Takahiro Ochiya[1]

[1]Department of Molecular and Cellular Medicine, Institute of Medical Science, Tokyo Medical University, Tokyo 160-0023, Japan.
[2]Department of Urology, Graduate School of Medicine, Chiba University, Chiba 260-8670, Japan.

Correspondence to: Prof. Takahiro Ochiya, Department of Molecular and Cellular Medicine, Institute of Medical Science, Tokyo Medical University, 6-7-1 Nishishinjuku, Shinjuku-ku, Tokyo 160-0023, Japan. E-mail: tochiya@tokyo-med.ac.jp

How to cite this article: Tamura T, Yoshioka Y, Ochiya T. Extracellular vesicles as the "magic bullet" for fighting threats to humanity. *Extracell Vesicles Circ Nucleic Acids* 2021;2:224-7. https://dx.doi.org/10.20517/evcna.2021.14

Received: 30 Jul 2021 **First Decision:** 25 Aug 2021 **Revised:** 30 Aug 2021 **Accepted:** 9 Sep 2021 **Available online:** 18 Sep 2021

Academic Editors: Yoke Peng Loh, Tsuneya Ikezu **Copy Editor:** Xi-Jun Chen **Production Editor:** Xi-Jun Chen

Abstract

Many researchers worldwide are currently trying to develop targeted molecular therapies such as nucleic acid medicines or antibody-drug conjugates for various diseases. Writing in *Extracellular Vesicles and Circulating Nucleic Acids*, Kim *et al.* summarized existing technologies for encapsulating therapeutic molecules into exosomes and introduced some human cell lines which are able to produce safe, effective therapeutic exosomes. Their review article offers the "magic bullet" for fighting threats to humanity such as the current coronavirus pandemic.

Keywords: Extracellular vesicles, therapeutic exosomes, drug delivery system, COVID-19

The "magic bullet" is a famous scientific idea advocated by Dr. Paul Ehrlich around 1900[1]. He was a German Nobel laureate, and he suggested that it could be possible to attack specific microbes which induce diseases without harming the body itself. He named this ideal agent a "magic bullet". Dr. Ehrlich's discovery in 1909 of arsphenamine for the treatment of syphilis is considered to be the first magic bullet. This finding led to the concept of therapeutic strategies for various diseases, including therapies against infections and chemotherapy. Many researchers worldwide are currently trying to develop targeted molecular therapies such as nucleic acid medicine or antibody-drug conjugates. However, the therapeutic effects of these treatments are still limited because it is difficult to deliver sufficient doses of a drug to a local lesion. For

clinical application, it is necessary to develop innovative drug delivery systems (DDSs) that can efficiently deliver drug molecules to a lesion. As Dr. Ehrlich pointed out, the materials used for this new delivery system need to be safe for our bodies.

Emerging evidence suggests that extracellular vesicles (EVs), such as exosomes, can be promising candidate materials for DDS. It was discovered in the mid-2000s that EVs containing miRNAs and mRNAs circulate in our bodies[2,3]. After this discovery, around 2010, it was shown that miRNAs encapsulated in EVs function in recipient cells[4-6]. In 2015, Zomer *et al.*[7] visualized intercellular molecular exchanges between tumor cells *in vivo* and showed that this phenomenon affects cellular metastatic behavior. These discoveries indicated that EVs play an active role in intercellular communication by transferring cellular materials to recipient cells, and they offer great potential as natural therapeutic delivery vehicles. Hoshino *et al.*[8] demonstrated that molecules present on tumor-derived exosomes allowed them to target specific organs. This directivity is considered to extend the possible uses of exosome-based magic bullets.

Dr. Chois' team is one of the leading research groups investigating exosome-based DDS and has made several contributions to this field. "EXPLOR", an optogenetically engineered exosome system capable of loading adequate doses of therapeutic proteins into exosomes, was developed by his group[9]. This review paper introduced some existing technologies for encapsulating therapeutic molecules into exosomes and discussed some human cell lines that produce exosomes, as promising materials for preparing safe therapeutic exosomes. They also discussed the use of naïve exosomes which produce their own therapeutic effects. It is desirable to use normal human cells or cell lines for preparing safe therapeutic agents, but there are several problems which still need to be considered. As Kim *et al.*[10] described in this review paper, scalability, consistency, and controllable manufacturing methods for culture will need to be established. Other sources of EVs have also been studied[11-14]. Some researchers previously studied the biological activities of bovine milk derived EVs (mEVs)[11], and they have reported novel methods for applying mEVs to drug delivery vehicles[12,13]. In these studies, they demonstrated that no adverse effect was observed after serial administration of mEVs in mice, and they found that bovine milk could be a scalable source of EVs for mass production[12,13]. Other researchers examined the feasibility of orally administered nucleic acid drug delivery by acerola exosome-like nanoparticles[14]. However, in terms of exosome engineering, human cells or cell lines would be the best source, because we can easily manipulate specific regulatory genes or proteins in exosome producing cells. The review by Kim *et al.*[10] is worthy of attention because the authors discuss these prospects and challenges for the clinical applications of exosome-based therapy in a straightforward manner.

To address the coronavirus pandemic, researchers worldwide are working on therapeutic approaches to COVID-19 using exosomes. Sengupta *et al.*[15] have conducted a prospective, nonrandomized, open-label cohort study, and have evaluated the safety and efficacy of commercially available exosomes (ExoFlo™) derived from allogeneic bone marrow mesenchymal stromal cells (BM-MSCs) as a treatment for severe COVID-19. The treatment resulted in significant improvement in absolute neutrophil count and lymphopenia, with a decline in C-reactive protein, ferritin, and D-dimers. This is one of the first published clinical studies to use BM-MSC-derived exosomes as a treatment for COVID-19[15]. Some researchers believe that RNA interference can serve as a genetic treatment approach for critically ill individuals with SARS-CoV-2. Owing to their natural characteristics, exosomes are considered to be suitable carriers for the delivery of interfering RNA. There have been attempts to produce MSC-derived exosomes carrying a cocktail of the RNAs which inhibit targets involved in SARS-CoV-2 pathogenesis for the treatment of COVID-19 patients[16].

Exosome-based therapies could be used in many types of diseases, including oncology and infectious diseases. The "EXPLORE" technology is innovative, and this kind of remarkable technology is based on deep insights into the biogenesis and delivery of exosomes. However, further insights and compliance with rigorous research and development guidelines are needed for clinical application. Recently, several significant position papers in this field have been provided to prevent any unproven EV therapies[17,18]. EV researchers need to follow the right path referring to these guide maps to overcome the immeasurable threats to humanity. These novel findings pave the way for future medical research, and we look forward to further development in this promising field.

DECLARATIONS

Authors' contributions

Made substantial contributions to conception, design, writing, and editing of the paper, and performed literature searches and interpretation: Tamura T, Yoshioka Y, Ochiya T

Availability of data and materials

Not applicable.

Financial support and sponsorship

None.

Conflicts of interest

All authors declared that there are no conflicts of interest.

Ethical approval and consent to participate

Not applicable.

Consent for publication

Not applicable.

REFERENCES

1. Tan SY, Grimes S. Paul Ehrlich (1854-1915): man with the magic bullet. *Singapore Med J* 2010;51:842-3. PubMed
2. Valadi H, Ekström K, Bossios A, Sjöstrand M, Lee JJ, Lötvall JO. Exosome-mediated transfer of mRNAs and microRNAs is a novel mechanism of genetic exchange between cells. *Nat Cell Biol* 2007;9:654-9. DOI PubMed
3. Ratajczak J, Miekus K, Kucia M, et al. Embryonic stem cell-derived microvesicles reprogram hematopoietic progenitors: evidence for horizontal transfer of mRNA and protein delivery. *Leukemia* 2006;20:847-56. DOI PubMed
4. Kosaka N, Iguchi H, Yoshioka Y, Takeshita F, Matsuki Y, Ochiya T. Secretory mechanisms and intercellular transfer of microRNAs in living cells. *J Biol Chem* 2010;285:17442-52. DOI PubMed PMC
5. Pegtel DM, Cosmopoulos K, Thorley-Lawson DA, et al. Functional delivery of viral miRNAs via exosomes. *Proc Natl Acad Sci U S A* 2010;107:6328-33. DOI PubMed PMC
6. Zhang Y, Liu D, Chen X, et al. Secreted monocytic miR-150 enhances targeted endothelial cell migration. *Mol Cell* 2010;39:133-44. DOI PubMed
7. Zomer A, Maynard C, Verweij FJ, et al. In vivo imaging reveals extracellular vesicle-mediated phenocopying of metastatic behavior. *Cell* 2015;161:1046-57. DOI PubMed PMC
8. Hoshino A, Costa-Silva B, Shen TL, et al. Tumour exosome integrins determine organotropic metastasis. *Nature* 2015;527:329-35. DOI PubMed PMC
9. Yim N, Ryu SW, Choi K, et al. Exosome engineering for efficient intracellular delivery of soluble proteins using optically reversible protein-protein interaction module. *Nat Commun* 2016;7:12277. DOI PubMed PMC
10. Kim J, Song Y, Park CH, Choi C. Platform technologies and human cell lines for the production of therapeutic exosomes. *Extracell Vesicles Circ Nucleic Acids* 2021;2:3-17. DOI
11. Samuel M, Chisanga D, Liem M, et al. Bovine milk-derived exosomes from colostrum are enriched with proteins implicated in

immune response and growth. *Sci Rep* 2017;7:5933. DOI PubMed PMC

12. Somiya M, Yoshioka Y, Ochiya T. Biocompatibility of highly purified bovine milk-derived extracellular vesicles. *J Extracell Vesicles* 2018;7:1440132. DOI PubMed PMC
13. Munagala R, Aqil F, Jeyabalan J, et al. Exosomal formulation of anthocyanidins against multiple cancer types. *Cancer Lett* 2017;393:94-102. DOI PubMed PMC
14. Umezu T, Takanashi M, Murakami Y, et al. Acerola exosome-like nanovesicles to systemically deliver nucleic acid medicine via oral administration. *Mol Ther Methods Clin Dev* 2021;21:199-208. DOI PubMed PMC
15. Sengupta V, Sengupta S, Lazo A, Woods P, Nolan A, Bremer N. Exosomes derived from bone marrow mesenchymal stem cells as treatment for severe COVID-19. *Stem Cells Dev* 2020;29:747-54. DOI PubMed PMC
16. Jamalkhah M, Asaadi Y, Azangou-Khyavy M, et al. MSC-derived exosomes carrying a cocktail of exogenous interfering RNAs an unprecedented therapy in era of COVID-19 outbreak. *J Transl Med* 2021;19:164. DOI PubMed PMC
17. Théry C, Witwer KW, Aikawa E, et al. Minimal information for studies of extracellular vesicles 2018 (MISEV2018): a position statement of the International Society for Extracellular Vesicles and update of the MISEV2014 guidelines. *J Extracell Vesicles* 2018;7:1535750. DOI PubMed PMC
18. Börger V, Weiss DJ, Anderson JD, et al. International Society for Extracellular Vesicles and International Society for Cell and Gene Therapy statement on extracellular vesicles from mesenchymal stromal cells and other cells: considerations for potential therapeutic agents to suppress coronavirus disease-19. *Cytotherapy* 2020;22:482-5. DOI PubMed PMC

Linthorst *et al. Extracell Vesicles Circ Nucleic Acids* 2021;2:228-37
DOI: 10.20517/evcna.2021.13

Extracellular Vesicles and Circulating Nucleic Acids

Original Article

Open Access

Check for updates

Distinct fragmentation patterns of circulating viral cell-free DNA in 83,552 non-invasive prenatal testing samples

Jasper Linthorst[1], Matthijs R. A. Welkers[2], Erik A. Sistermans[1]

[1]Department of Human Genetics and Amsterdam Reproduction & Development research institute, Amsterdam UMC, Vrije Universiteit Amsterdam, Amsterdam 1081 BT, The Netherlands.
[2]Department of Medical Microbiology & Infection Prevention, Amsterdam UMC, Amsterdam 1081 BT, The Netherlands.

Correspondence to: Dr. Erik A. Sistermans, Department of Human Genetics and Amsterdam Reproduction & Development research institute, Amsterdam UMC, Vrije Universiteit Amsterdam, van der Boechorststraat 7, Amsterdam 1081 BT, The Netherlands. E-mail: e.sistermans@amsterdamumc.nl

How to cite this article: Linthorst J, Welkers MRA, Sistermans EA. Distinct fragmentation patterns of circulating viral cell-free DNA in 83,552 non-invasive prenatal testing samples. *Extracell Vesicles Circ Nucleic Acids* 2021;2:228-37. https://dx.doi.org/10.20517/evcna.2021.13

Received: 19 Jul 2021 **First Decision:** 25 Aug 2021 **Revised:** 13 Sep 2021 **Accepted:** 27 Sep 2021 **Available online:** 30 Sep 2021

Academic Editors: Yoke Peng Loh, Michael Graner **Copy Editor:** Xi-Jun Chen **Production Editor:** Xi-Jun Chen

Abstract

Aim: The fragmentation characteristics of cell-free DNA (cfDNA) are informative biomarkers in liquid biopsies, including non-invasive prenatal testing (NIPT), as they provide insights into the origins of the cfDNA. Viral infections by DNA viruses can contribute to the available cfDNA in these samples. Here, we characterize the fragment size distribution of viral cfDNA fragments obtained from available anonymous NIPT samples.

Methods: A viral database of 224 DNA viruses was generated from the NCBI RefSeq viral database. Paired-end cfDNA sequencing reads from 83.522 NIPT samples that did not map to any of the human chromosomes, or mitochondrial DNA of the human reference genome build GRCh38 (excluding alternative and unplaced contigs) were remapped to the generated viral database. Reads mapping to the 14 most abundant DNA viruses were selected, and fragment size distributions were analyzed in detail.

Results: Distinct fragmentation patterns were identified for several DNA viruses, most likely due to differences in viral tropism, chromatinization (binding of nucleosomes), and the topology of the viral DNA. In high viral load parvo B19 positive samples, the fragment size distribution differed between samples, potentially reflecting the state of the infection.

Conclusion: These findings outline the potential for liquid biopsies to elucidate the dynamics behind the viral infection, which may potentially have various clinical applications. Our data provide preliminary insights on the use of fragmentomics of viral cfDNA to distinguish between reactivation, reinfection, and primary infection and monitoring the state of viral infections.

Keywords: Virome, fragmentomics, DNA degradation, epigenetics, viral cell-free DNA, NIPT

INTRODUCTION

Non-invasive prenatal testing (NIPT) in pregnant women can be performed by untargeted whole genome sequencing of cell-free DNA (cfDNA). While cfDNA predominantly stems from chromosomal DNA of apoptotic blood cells[1], small amounts of viral cfDNA can also be detected in NIPT samples[2]. As cfDNA is not sheared before sequencing, the insert size of a paired-end sequencing read can be used to determine the actual size of the cfDNA fragments[3]. In maternal blood plasma, most cfDNA fragments of fetal (placental) origin are 147bp (the size of a nucleosome), while most fragments of maternal origin are 166bp (the size of a nucleosome + the h1 linker histone, named a chromatosome)[4]. During genome deconstruction of apoptotic cells, nucleosomes impede endonuclease activity causing most chromosomal cfDNA fragments to be the size of approximately a nucleosome. This characteristic size distribution is predominantly driven by the nucleosome occupancy of the underlying apoptotic cells. This is confirmed by the different size distribution of cell-free mitochondrial DNA, which is known to be free of nucleosomes and does not show any increase in nucleosome-sized fragments[1]. These molecular characteristics of cfDNA, termed fragmentomics, are also used in liquid biopsies (such as NIPT) to estimate the fraction of placenta-derived DNA in a sample[5] or in cancer diagnosis to detect marks of aberrant epigenetic regulation[6].

Infectious viral DNA is packaged in virions in which the genome is protected by a capsid structure free of nucleosomes[7]. Upon infecting a cell, the viral DNA is rapidly loaded with histones to suppress viral gene expression[7]. Although this form of "epigenetic silencing" inhibits viral gene expression and initially prevents the spread of the infection, it also enables the virus to evade the host immune system and establish a latent infection. Studies have also shown that the nucleosome positioning on viral DNA within the nucleus of infected cells is dynamic, non-random, and presumably plays a vital role in the lifecycle of the virus[7-9].

Viral cfDNA fragments, as sequenced by cfDNA sequencing, are naturally degraded short fragments of DNA. They are expected to result from either (latently) infected apoptotic cells or degraded virions. Therefore, the detection of viral sequences in cfDNA is no direct evidence of a productive viral infection. However, the size distribution of the viral cfDNA fragments may provide clues as to whether (or what fraction of) the originating viral genomes were infectious or not. This is based on the assumption that nucleosome-bound viral cfDNA stems from apoptotic infected cells, while nucleosome-free viral cfDNA stems from virion DNA.

Previously it was shown that both virion-associated Parvovirus B19 and non-infectious "naked" Parvovirus B19 DNA could be detected from blood samples of asymptomatic blood donors. In addition, exogenous treatment with endonucleases could be used to distinguish infectious from non-infectious parvovirus B19 DNA[10]. Similarly, for Epstein-Barr virus (EBV), it was shown that both "naked" and virion-associated DNA could be detected in plasma and that depending on the type of EBV-associated disease, the combination of the two differed[11]. It has also been shown that the fragment size distribution of EBV is an informative biomarker for the early detection of nasopharyngeal cell carcinoma (NPC) from liquid biopsies using

cfDNA sequencing[12,13]. Longer, assumed nucleosome bound, circulating EBV fragments were more frequently observed in NPC cases than non-NPC cases. In a different study[14], circulating cytomegalovirus cfDNA was shown to be exceptionally fragmented, explaining discrepancies in viral load estimates between PCR and NGS-based detection methods, as in PCR, the primers could be too widely spaced to detect the short fragments. Furthermore, the median CMV fragment length was shorter in NIPT samples than cfDNA from transplant patients who had higher viral loads on average. One explanation for these differences was that they were suspected to arise from differences in the epigenetic state of the circulating CMV or the state of reactivation.

Here we explore the fragment size distributions of the 14 most abundant DNA viruses in our dataset. The cfDNA fragments were extracted from 83.552 NIPT samples.

METHODS

Data

De-identified cell-free paired-end cfDNA sequencing data was used from NIPT analyses handled by the Amsterdam UMC between June 2018 and December 2020, and all samples were processed using the VeriSeq method (Illumina, San Diego, USA). Upon isolation of cfDNA, samples were paired-end sequenced using 36bp on an Illumina NextSeq500. Raw base call files were de-multiplexed, and adapters were trimmed using bcl2fastq (2.17.1.14), resulting in, on average, ~22.5 million reads per sample.

Viral database construction and grouping of viral genomes

From the NCBI RefSeq viral database, 224 human host DNA viruses (excluding RNA retroviruses) were selected [Supplementary Table 1] and combined into a single viral reference dataset. We applied the DUST algorithm as implemented in the meme-suite[15] (version 5.3) with default settings to mask regions of low-complexity sequence to prevent spurious alignments. Highly identical reference assemblies were grouped using the NCBI taxonomy database and assigned to specific virus groups [Supplementary Table 1].

In order to query the database, the ETE3 python package[16] was used. Next, distances between reference assemblies were computed using Mash[17], and ambiguous alignments were inspected using the XA tag reported by BWA[18]. Finally, groups of highly identical genomes were linked to knots in the taxonomic tree and labeled accordingly. Knots were chosen such that the number of ambiguously positioned reads that exceed group boundaries would be minimized.

Extraction and alignment of unmapped reads

Reads that did not map to the human genome (build GRCh38; excluding alt, random and unplaced sequence) were extracted from the samples using Samtools (-f 4)[19]. All unmapped reads were subsequently aligned to our database of viral genomes using BWA mem[20] (version 0.7.17), and duplicate reads were marked (and later discarded in further analyses) using Samblaster[21].

Viruses for which more than 100 paired-end reads could be mapped in the correct orientation were used to model fragment-size distributions [Supplementary Table 2]. Fragment sizes were derived from the "template length" field as calculated by pysam (https://github.com/pysam-developers/pysam). There was no correlation between the size of the viral genome and the number of aligned reads (Spearman $r = 0.24$, $P = 0.33$; Pearson $r = 0.24$, $P = 0.34$).

Fetal fraction

The fraction of fetal cfDNA within the sequenced maternal plasma was calculated using the SeqFF method[22].

Data processing

All non-duplicate reads aligned to our viral reference database were merged into a single cram[23]. Then, fragment sizes were calculated, and reads were linked to the input samples through the attached read group tags. Data analysis and plotting were performed using Python and the libraries Pysam, Seaborn (0.11.0), Pandas (1.1.1), Numpy (1.19.5), and Scipy (1.6.0).

RESULTS

A total of 139,573 read pairs of suspected viral origin were detected across 13,314 NIPT samples of unique pregnancies. Per NIPT sample, we generally detect a small number of reads of suspected viral origin (for details, see Supplementary Table 2). However, by pooling this data, we obtained sufficient fragments to investigate the fragment size distributions of 14 viral species and compared it to the size distribution of human chromosome and mitochondrial-derived cfDNA [Figure 1]. Except for human herpesvirus 6 (HHV6), the fragment size distributions of all DNA viruses were highly distinct from that of chromosomal cfDNA. For adenovirus, adeno-associated virus (AAV), herpes simplex virus (HSV), and varicella-zoster virus (VZV), only very short viral cfDNA fragments were observed with no increase in the number of nucleosome-sized fragments; comparable to what is seen for mitochondrial cfDNA. The fragment size distribution of HHV6 seemed to exactly overlap with that of chromosomal cfDNA, indicating that the majority of the sequenced HHV6 fragments originated from the inherited chromosomally integrated HHV6 viruses (iciHHV6)[24], which is known to be present on 0.5% of human alleles. The abundance of HHV6 fragments across all NIPT samples followed a trimodal distribution [Figure 2A] which most likely reflects that the iciHHV6 genotype of the mother and fetus contributes most of the HHV6 reads in samples with a high or intermediate HHV6 abundance. In samples with intermediate HHV6 abundance, the abundance correlated with the calculated fetal fraction, in line with germline integration of HHV6 on the paternal allele in the genome of the fetus [Figure 2B]. Although this indicates that genotyping paternally inherited fetal iciHHV6 from NIPT sequencing seems feasible, we did not study maternally inherited iciHHV6 or potential HHV6 integration copy-number differences. In addition, the modes of the fragment size distributions of intermediate and high HHV6 abundant samples exactly overlapped with the size distributions of fetal (peaks around the size of a single nucleosome: 143bp) and maternal (peaks around the size of a chromatosome: 166bp) chromosomal cfDNA respectively [Figure 2C]. The fragment size distribution of samples with a low abundance was significantly different (Kolmogorov Smirnoff test, $P = 3.74e\text{-}17$) from the size distribution of samples with an intermediate HHV6 abundance and contained more HHV6 fragments in the size range of 50-100bp. Indicative of the fact that in low abundant HHV6 samples, viral fragments were observed that originated from unchromatinized not chromosomally integrated viral cfDNA, possibly from degraded HHV6 virions.

Further direct evidence for these results follows from the viral chimeric reads, for which one end aligns to the human genome and the other to a viral genome. For many of these reads, we found that the end that maps to the human genome has an extreme GC content (> 85%) which are predominantly aligned to a G-homopolymer on chromosome 2. This resulted in a very different GC content between the human and viral end of the two pairs. The origin of this bias is unclear but may be caused by errors in sequencing of, for example, very short or perhaps single-stranded cfDNA fragments. After excluding the chimeric reads for which the human end had a GC content of above 85%, we found 113 reads for which one end mapped to the human genome and the other end mapped to HHV6. These reads all originated from samples with an intermediate (5) and high (108) abundance of HHV6. However, as HHV6 is also known to integrate its genome into the telomeres of infected somatic cells, we cannot exclude that such reads cannot be observed from low-abundant HHV6 samples. Furthermore, as HHV6 preferably integrates into the telomeres of human chromosomes, it is somewhat complicated to accurately position them on the human genome, as the telomeric sequence is highly repetitive and occurs on all chromosomes. Presumably, for this reason, we

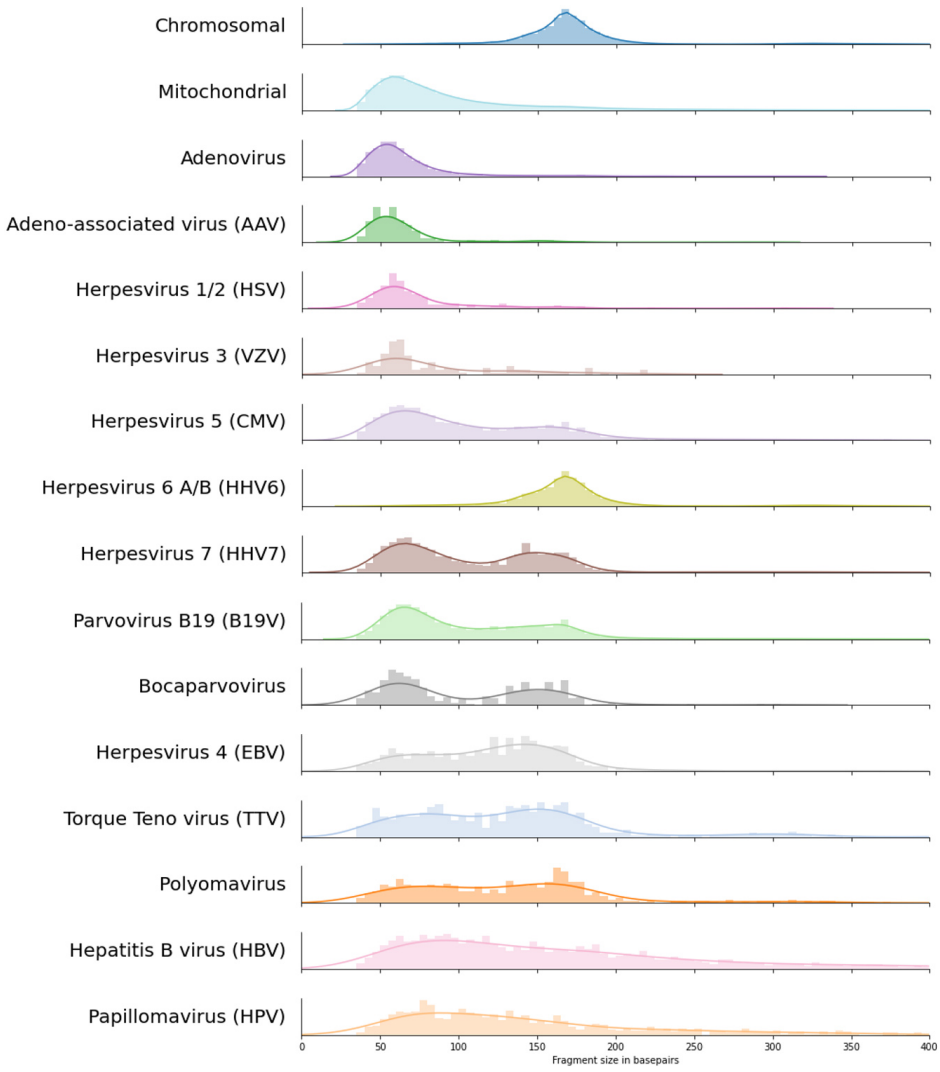

Figure 1. cfDNA fragment length density distributions for the 14 viruses with most paired viral reads with on top the typical human cfDNA fragment length density distribution. Colors are transferred from Figure 2, and viruses are sorted by the total number of paired viral reads that were used to estimate the fragment length densities; bin sizes are adjusted according to the total number of observed paired reads. cfDNA: Cell-free DNA.

found that the 113 chimeric HHV6 reads were distributed across almost all human chromosomes.

Bimodal size distributions were observed for the other two betaherpesviruses, CMV (HHV5) and HHV7. The first peak of the distribution is observed at ~60bp, similar to mitochondrial cfDNA fragments. The second less pronounced peak is around 150bp, slightly shorter than chromosomal cfDNA, possibly indicating that both nucleosome-bound and unbound viral cfDNA are observed in blood plasma. For Bocaparvoviruses and Parvovirus B19, a similar bimodality can be observed [Figure 1]. Three samples with a (suspected) acute infection had an extraordinarily high viral load of Parvovirus B19, with between 3000 and 6000 viral reads per sample. By inspecting the fragment size distributions of these individual samples, we found that they varied between samples and that both short and long cfDNA fragments were present within all samples [Figure 3].

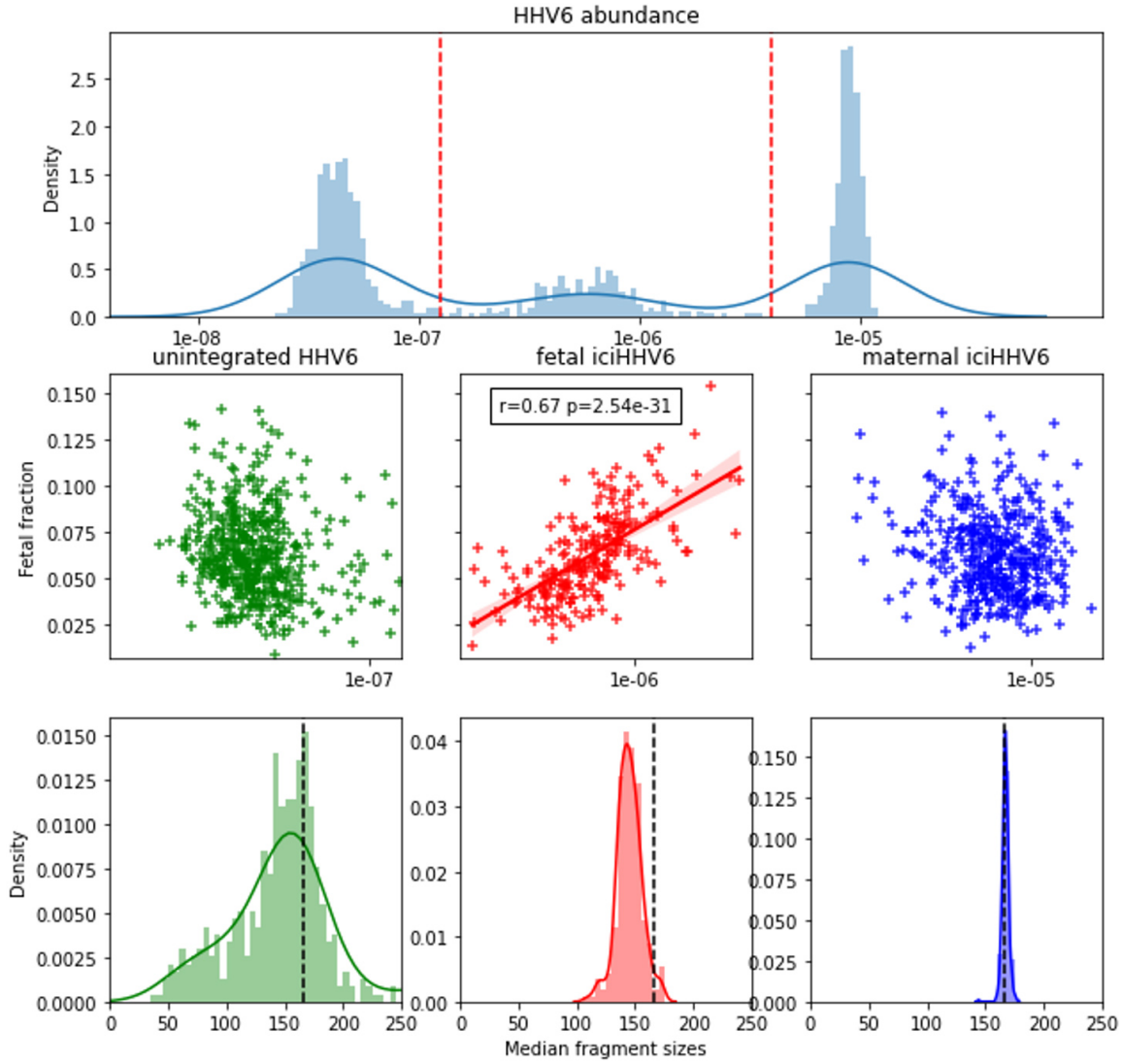

Figure 2. The abundance of HHV6 distinguishes (paternally inherited) fetal and maternal iciHHV6 and shows differing characteristic fragment size distributions. (A) Distributions of HHV6 abundance expressed as the number of viral HHV6 fragments divided over the total number of chromosomal fragments across all HHV6 positive samples on the x-asix. The y-axis represents a histogram (light blue bars) paired with kernel density estimation (dark blue line). Red dashed vertical lines indicate how samples are grouped into low (unintegrated/inherited HHV6; *n* = 479), intermediate (paternally inherited fetal iciHHV6; *n* = 226), and high (maternal iciHHV6; *n* = 441) abundance. (B) Scatter plots indicating the correlation between the calculated fetal fraction of a NIPT sample (y-axis) and the HHV6 abundance (x-axis). A significant correlation is only observed between the calculated fetal fraction and fetal iciHHV6 (red). (C) Different size distributions are observed for the three groups. Typical size distributions are observed with a peak of 143bp for fetal chromosomal cfDNA (red) and maternal cfDNA (blue). The presumed non-iciHHV6 fragments exhibit an increased frequency of short (50bp-100bp) cfDNA fragments. The dashed black line in all three figures indicates the typical 166bp fragment size of chromosomal cfDNA. HHV6: Human herpesvirus 6; iciHHV6: inherited chromosomally integrated HHV6 viruses; NIPT: non-invasive prenatal testing; cfDNA: cell-free DNA.

Finally, the size distribution of viral fragments from circular viruses [torque-tenovirus (TTV), human papillomavirus (HPV), hepatitis B virus (HBV), and Polyomaviruses] was significantly different from those of linear viruses (Adenovirus, AAV, HSV, VZV, CMV, HHV7, B19V, EBV) (Kolmogorov Smirnoff test, P = 1.68e-198). The median fragment size of circular viruses was 133bp, while the median fragment size of linear viruses was only 87bp. For TTV and Polyomavirus, fragment sizes are widely distributed, with slightly more fragments around the size of a single nucleosome. For HPV and HBV, we observe a random

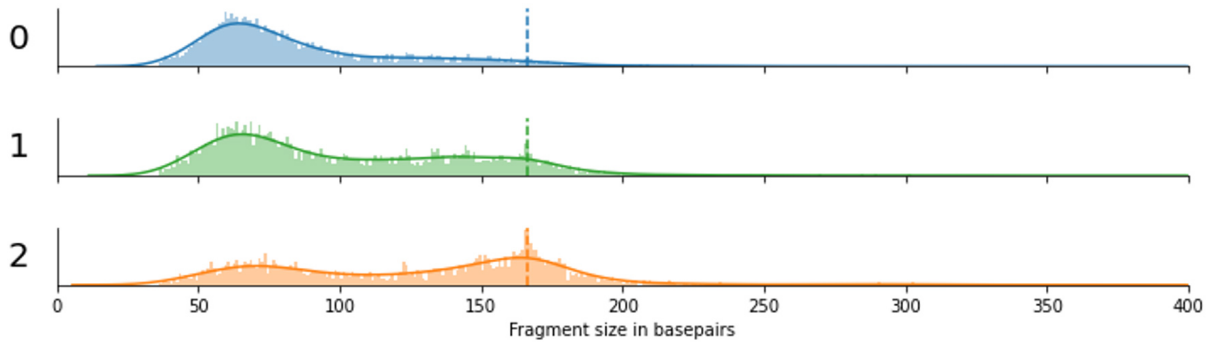

Figure 3. Fragment size distributions of three independent cases (labeled 0, 1, and 2) with a high viral load of Parvovirus B19. The dashed line indicates the 166bp peak that is observed for chromosomally derived cell-free DNA fragments.

distribution of fragment sizes without any apparent increase in nucleosome-sized fragments, similar to alphaherpesviruses, adenoviruses, and mitochondrial cfDNA, but consisting of longer fragments.

DISCUSSION

Fragmentation patterns of cell-free plasma DNA are essential biomarkers in the rapidly increasing field of liquid biopsies. Therefore, we studied the fragmentation patterns of viral plasma DNA, obtained from 83.552 mostly healthy pregnant women, and demonstrated specific variations between different viruses and presumably during specific infections.

In general, we observe different types of size distributions that can be related to different forms of viral infections compared with other cfDNA types. Size distribution of viral cfDNA fragments in the size range of 130bp to 170bp is comparable to cfDNA from chromosomal cfDNA where the size distribution is known to depend on nucleosome binding. As a consequence, this size distribution of viral cfDNA might be the result of nucleosomes that bind the viral DNA, presumably as part of the host innate immune response to inhibit viral gene expression, or because the viral DNA was integrated into the genomic DNA, as is the case for HHV6. In analogy with cfDNA fragmentation of nucleosome-free mitochondrial cfDNA, shorter viral cfDNA fragments are expected to stem from nucleosome-free viral DNA. Possible sources could be degraded virions or replicating DNA from active infections.

The bimodal distributions observed for a select subset of viruses might indicate that cell tropism, model of latency, and/or the immune response to these viruses are differently regulated. We hypothesize that, as different viruses target different cell-types and cell-types differentially contribute to the composition of cfDNA in plasma (a property used in tumor liquid biopsies to determine the cell-type of origin[6]), this may influence the number of the observed nucleosome bound viral fragments based on the viral species. For example, CMV, EBV, HHV6, HHV7, and Parvovirus B19 predominantly infect (and achieve latency) hematopoietic progenitor cells and leukocytes, which are all essential contributors to cfDNA in blood plasma. This contrasts to HPV, HBV, Adeno, VZV, and HSV, which mainly target epithelial, endothelial, and nerve cells, cell types that contribute less to the pool of circulating cfDNA in blood plasma, which might explain the presence of a nucleosome-bound peak in the first group, and its absence in the latter group of viruses.

Interestingly, in three cases with a high viral load of parvovirus B19 DNA, suggestive of an active or more recent infection, we observe that within these samples, both short (< 100bp) and long (nucleosome-sized) fragments co-occur and that the frequency with which they occur is highly variable between samples. We

suspect that this could be representative of the number of circulating virions (short fragments) *vs.* the number of infected cells (nucleosome-sized fragments), which in turn may represent the differential timing of sampling within these active infections.

The size distribution of viral fragments originating from circular viruses was significantly different from that of linear viruses. The median fragment size from circular viruses was larger than that of linear viruses, possibly reflecting the protection of circular DNA from exonuclease activity[1].

The observed variation in viral fragment sizes has consequences for the design of accurate quantitative PCR-based assays[25]. As many fragments are very small, primer-pairs used for PCR should not be widely spaced to prevent missing these fragments.

In this work, we found that on a per-sample basis, very little viral fragments were sequenced. Possibly this is due to the double-stranded library preparation protocol was used, as previous work has shown that single-stranded library preparation can significantly increase the number of sequenced viral fragments in plasma DNA. Future work should address whether our findings can be replicated with a single-stranded DNA library preparation protocol, as this could significantly improve the potential of viral plasma DNA sequencing on a per-sample basis.

In summary, we have shown that sequenced viral cfDNA fragments that were extracted from a large pool of NIPT sequencing data exhibit virus-specific size distributions, which are non-random and mostly distinct from typical chromosomal cfDNA. The mechanisms that give rise to these patterns are largely unknown, but our data link it to viral tropism, chromatinization, and the topology of the viral DNA. Further research is needed to evaluate how these characteristics of circulating viral cfDNA can be used in a clinical setting. Preliminary studies have been started in our center.

DECLARATIONS

Acknowledgements

The authors like to thank the Core Facility Genomics, and especially Dr. Daoud Sie, for providing compute and assistance with collecting data. All participating women in the TRIDENT-2 study are thanked for allowing us to use data for research in the further development of NIPT. We thank the NIPT consortium for building the study we could base our analysis on.

Authors' contributions

Study design, data analyses and wrote the manuscript: Linthorst J
Co-authored the manuscript and consultation on virology: Welkers MRA
Co-authored the manuscript and supervised the work: Sistermans EA

Availability of data and materials

Not applicable.

Financial support and sponsorship

None.

Conflicts of interest

All authors declared that there are no conflicts of interest.

Ethical approval and consent to participate

Research involving human subjects, human material or human data was performed in accordance with the Declaration of Helsinki. Approval for the TRIDENT study was granted by the Dutch Ministry of Health, Welfare, and Sport (license 1017420-153371-PG) and the Medical Ethical Committee of VU University Medical Center Amsterdam (No. 2017.165). Written informed consent to participate in TRIDENT-2 was obtained from all participating women. Approval for the anonymous use of NIPT data for viral analysis is pending.

Consent for publication

Not applicable.

REFERENCES

1. Lo YMD, Han DSC, Jiang P, Chiu RWK. Epigenetics, fragmentomics, and topology of cell-free DNA in liquid biopsies. *Science* 2021;372:eaaw3616. DOI PubMed
2. Liu S, Huang S, Chen F, et al. Genomic analyses from non-invasive prenatal testing reveal genetic associations, patterns of viral infections, and Chinese population history. *Cell* 2018;175:347-359.e14. DOI PubMed
3. Lo YM, Chan KC, Sun H, et al. Maternal plasma DNA sequencing reveals the genome-wide genetic and mutational profile of the fetus. *Sci Transl Med* 2010;2:61ra91. DOI PubMed
4. Kohabir K, Wolthuis R, Sistermans EA. Fragmentomic cfDNA patterns in noninvasive prenatal testing and beyond. *J Biomed Transl Res* 2021;7:38-47. DOI
5. Yu SC, Chan KC, Zheng YW, et al. Size-based molecular diagnostics using plasma DNA for noninvasive prenatal testing. *Proc Natl Acad Sci U S A* 2014;111:8583-8. DOI PubMed PMC
6. der Pol Y, Mouliere F. Toward the early detection of cancer by decoding the epigenetic and environmental fingerprints of cell-free DNA. *Cancer Cell* 2019;36:350-68. DOI PubMed
7. Tsai K, Cullen BR. Epigenetic and epitranscriptomic regulation of viral replication. *Nat Rev Microbiol* 2020;18:559-70. DOI PubMed PMC
8. Zalckvar E, Paulus C, Tillo D, et al. Nucleosome maps of the human cytomegalovirus genome reveal a temporal switch in chromatin organization linked to a major IE protein. *Proc Natl Acad Sci U S A* 2013;110:13126-31. DOI PubMed PMC
9. Oh J, Sanders IF, Chen EZ, et al. Genome wide nucleosome mapping for HSV-1 shows nucleosomes are deposited at preferred positions during lytic infection. *PLoS One* 2015;10:e0117471. DOI PubMed PMC
10. Backer MW, Russcher A, Kroes AC, Koppelman MH, Lanfermeijer M, Zaaijer HL. Detection of parvovirus B19 DNA in blood: viruses or DNA remnants? *J Clin Virol* 2016;84:19-23. DOI PubMed
11. Ryan JL, Fan H, Swinnen LJ, et al. Epstein-Barr virus (EBV) DNA in plasma is not encapsidated in patients with EBV-related malignancies. *Diagn Mol Pathol* 2004;13:61-8. DOI PubMed
12. Lam WKJ, Jiang P, Chan KCA, et al. Sequencing-based counting and size profiling of plasma Epstein-Barr virus DNA enhance population screening of nasopharyngeal carcinoma. *Proc Natl Acad Sci U S A* 2018;115:E5115-24. DOI PubMed PMC
13. Lam WKJ, Jiang P, Chan KCA, et al. Methylation analysis of plasma DNA informs etiologies of Epstein-Barr virus-associated diseases. *Nat Commun* 2019;10:3256. DOI PubMed PMC
14. Peddu V, Bradley BT, Casto AM, et al. High-resolution profiling of human cytomegalovirus cell-free DNA in human plasma highlights its exceptionally fragmented nature. *Sci Rep* 2020;10:3734. DOI PubMed PMC
15. Bailey TL, Boden M, Buske FA, et al. MEME SUITE: tools for motif discovery and searching. *Nucleic Acids Res* 2009;37:W202-8. DOI PubMed PMC
16. Huerta-Cepas J, Serra F, Bork P. ETE 3: reconstruction, analysis, and visualization of phylogenomic data. *Mol Biol Evol* 2016;33:1635-8. DOI PubMed PMC
17. Ondov BD, Treangen TJ, Melsted P, et al. Mash: fast genome and metagenome distance estimation using MinHash. *Genome Biol* 2016;17:132. DOI PubMed PMC
18. Li H. Aligning sequence reads, clone sequences and assembly contigs with BWA-MEM. Available from: https://arxiv.org/abs/1303.3997. [Last accessed on 28 Sep 2021].
19. Li H, Handsaker B, Wysoker A, et al; 1000 Genome Project Data Processing Subgroup. The sequence alignment/map format and SAMtools. *Bioinformatics* 2009;25:2078-9. DOI PubMed PMC
20. Li H, Durbin R. Fast and accurate long-read alignment with Burrows-Wheeler transform. *Bioinformatics* 2010;26:589-95. DOI PubMed PMC
21. Faust GG, Hall IM. SAMBLASTER: fast duplicate marking and structural variant read extraction. *Bioinformatics* 2014;30:2503-5. DOI PubMed PMC

22. Kim SK, Hannum G, Geis J, et al. Determination of fetal DNA fraction from the plasma of pregnant women using sequence read counts. *Prenat Diagn* 2015;35:810-5. DOI PubMed
23. Fritz M, Leinonen R, Cochrane G, Birney E. Efficient storage of high throughput DNA sequencing data using reference-based compression. *Genome Res* 2011;21:734-40. DOI PubMed PMC
24. Pantry SN, Medveczky PG. Latency, Integration, and reactivation of human herpesvirus-6. *Viruses* 2017;9:194. DOI PubMed PMC
25. Cook L, Starr K, Boonyaratanakornkit J, Hayden R, Sam SS, Caliendo AM. Does size matter? *J Clin Microbiol* 2018;56:e01061-18. DOI PubMed PMC

AUTHOR INSTRUCTIONS

1. Submission Overview

Before you decide to publish with *Extracellular Vesicles and Circulating Nucleic Acids* (*EVCNA*), please read the following items carefully and make sure that you are well aware of Editorial Policies and the following requirements.

1.1 Topic Suitability

The topic of the manuscript must fit the scope of the journal. Please refer to Aims and Scope for more information.

1.2 Open Access and Copyright

The journal adopts Gold Open Access publishing model and distributes content under the Creative Commons Attribution 4.0 International License. Copyright is retained by authors. Please make sure that you are well aware of these policies.

1.3 Publication Fees

The publication fee for each submission is $299. There are no additional charges based on color, length, figures, or other elements. OAE provides expense deduction for authors as appropriate. For more details, please refer to OAE Publication Fees.

1.4 Language Editing

All submissions are required to be presented clearly and cohesively in good English. Authors whose first language is not English are advised to have their manuscripts checked or edited by a native English speaker before submission to ensure the high quality of expression. A well-organized manuscript in good English would make the peer review even the whole editorial handling more smoothly and efficiently.

If needed, authors are recommended to consider the language editing services provided by Charlesworth to ensure that the manuscript is written in correct scientific English before submission. Authors who publish with OAE journals enjoy a special discount for the services of Charlesworth via the following two ways.

Submit your manuscripts directly at http://www.charlesworthauthorservices.com/~OAE;

Open the link http://www.charlesworthauthorservices.com/, and enter Promotion Code "OAE" when you submit.

1.5 Work Funded by the National Institutes of Health

If an accepted manuscript was funded by National Institutes of Health (NIH), the authors may inform Editors of the NIH funding number. The Editors are able to deposit the paper to the NIH Manuscript Submission System on behalf of the authors.

2. Submission Preparation

2.1 Cover Letter

A cover letter is required to be submitted accompanying each manuscript. It should be concise and explain why the study is significant, why it fits the scope of the journal, and why it would be attractive to readers, *etc*.

Here is a guideline of a cover letter for authors' consideration:

In the first paragraph: include the title and type (e.g., Original Article, Review, Case Report, *etc*.) of the manuscript, a brief on the background of the study, the question the author sought out to answer and why;

In the second paragraph: concisely explain what was done, the main findings and why they are significant;

In the third paragraph: indicate why the manuscript fits the Aims and Scope of the journal, and why it would be attractive to readers;

In the fourth paragraph: confirm that the manuscript has not been published elsewhere and not under consideration of any other journal. All authors have approved the manuscript and agreed on its submission to the journal. Journal's specific requirements have been met if any.

If the manuscript is contributed to a special issue, please also mention it in the cover letter.

If the manuscript was presented partly or entirely in a conference, the author should clearly state the background information of the event, including the conference name, time and place in the cover letter.

2.2 Types of Manuscripts

There is no restriction on the length of manuscripts, number of figures, tables and references, provided that the manuscript is concise and comprehensive. The journal publishes Original Article, Review, Meta-Analysis, Case Report, Commentary, *etc*. For more details about paper type, please refer to the following table.

Manuscript Type	Definition	Abstract	Keywords	Main Text Structure
Original Article	An Original Article describes detailed results from novel research. All findings are extensively discussed.	Structured abstract including Aim, Methods, Results and Conclusion. No more than 250 words.	3-8 keywords	The main content should include four sections: Introduction, Methods, Results and Discussion.
Review	A Review paper summarizes the literature on previous studies. It usually does not present any new information on a subject.	Unstructured abstract. No more than 250 words.	3-8 keywords	The main text may consist of several sections with unfixed section titles. We suggest that the author includes an "Introduction" section at the beginning, several sections with unfixed titles in the middle part, and a "Conclusion" section in the end.
Case Report	A Case Report details symptoms, signs, diagnosis, treatment, and follows up an individual patient. The goal of a Case Report is to make other researchers aware of the possibility that a specific phenomenon might occur.	Unstructured abstract. No more than 150 words.	3-8 keywords	The main text consists of three sections with fixed section titles: Introduction, Case Report, and Discussion.
Meta-Analysis	A Meta-Analysis is a statistical analysis combining the results of multiple scientific studies. It is often an overview of clinical trials.	Structured abstract including Aim, Methods, Results and Conclusion. No more than 250 words.	3-8 keywords	The main content should include four sections: Introduction, Methods, Results and Discussion.
Systematic Review	A Systematic Review collects and critically analyzes multiple research studies, using methods selected before one or more research questions are formulated, and then finding and analyzing related studies and answering those questions in a structured methodology.	Structured abstract including Aim, Methods, Results and Conclusion. No more than 250 words.	3-8 keywords	The main content should include four sections: Introduction, Methods, Results and Discussion.
Technical Note	A Technical Note is a short article giving a brief description of a specific development, technique or procedure, or it may describe a modification of an existing technique, procedure or device applied in research.	Unstructured abstract. No more than 250 words.	3-8 keywords	/
Commentary	A Commentary is to provide comments on a newly published article or an alternative viewpoint on a certain topic.	Unstructured abstract. No more than 250 words.	3-8 keywords	/
Editorial	An Editorial is a short article describing news about the journal or opinions of senior editors or the publisher.	None required	None required	/
Letter to Editor	A Letter to Editor is usually an open post-publication review of a paper from its readers, often critical of some aspect of a published paper. Controversial papers often attract numerous Letters to Editor	Unstructured abstract (optional). No more than 250 words.	3-8 keywords (optional)	/
Opinion	An Opinion usually presents personal thoughts, beliefs, or feelings on a topic.	Unstructured abstract (optional). No more than 250 words.	3-8 keywords	/
Perspective	A Perspective provides personal points of view on the state-of-the-art of a specific area of knowledge and its future prospects. Links to areas of intense current research focus can also be made. The emphasis should be on a personal assessment rather than a comprehensive, critical review. However, comments should be put into the context of existing literature. Perspectives are usually invited by the Editors.	Unstructured abstract. No more than 150 words.	3-8 keywords	/

2.3 Manuscript Structure

2.3.1 Front Matter

2.3.1.1 Title

The title of the manuscript should be concise, specific and relevant, with no more than 16 words if possible. When gene or protein names are included, the abbreviated name rather than full name should be used.

2.3.1.2 Authors and Affiliations

Authors' full names should be listed. The initials of middle names can be provided. Institutional addresses and email addresses for all authors should be listed. At least one author should be designated as corresponding author. In addition, corresponding authors are suggested to provide their Open Researcher and Contributor ID upon submission. Please note that any change to authorship is not allowed after manuscript acceptance.

2.3.1.3 Abstract

The abstract should be a single paragraph with word limitation and specific structure requirements (for more details please refer to Types of Manuscripts). It usually describes the main objective(s) of the study, explains how the study was done, including any model organisms used, without methodological detail, and summarizes the most important results and their significance. The abstract must be an objective representation of the study: it is not allowed to contain results which are not presented and substantiated in the manuscript or exaggerate the main conclusions. Citations should not be included in the abstract.

2.3.1.4 Keywords

Three to eight keywords should be provided, which are specific to the article, yet reasonably common within the subject discipline.

2.3.2 Main Text

Manuscripts of different types are structured with different sections of content. Please refer to Types of Manuscripts to make sure which sections should be included in the manuscripts.

2.3.2.1 Introduction

The introduction should contain background that puts the manuscript into context, allow readers to understand why the study is important, include a brief review of key literature, and conclude with a brief statement of the overall aim of the work and a comment about whether the aim was achieved. Relevant controversies or disagreements in the field should be introduced as well.

2.3.2.2 Methods

Methods should contain sufficient details to allow others to fully replicate the study. New methods and protocols should be described in detail while well-established methods can be briefly described or appropriately cited. Experimental participants selected, the drugs and chemicals used, the statistical methods taken, and the computer software used should be identified precisely. Statistical terms, abbreviations, and all symbols used should be defined clearly. Protocol documents for clinical trials, observational studies, and other non-laboratory investigations may be uploaded as supplementary materials.

2.3.2.3 Results

This section contains the findings of the study. Results of statistical analysis should also be included either as text or as tables or figures if appropriate. Authors should emphasize and summarize only the most important observations. Data on all primary and secondary outcomes identified in the section Methods should also be provided. Extra or supplementary materials and technical details can be placed in supplementary documents.

2.3.2.4 Discussion

This section should discuss the implications of the findings in context of existing research and highlight limitations of the study. Future research directions may also be mentioned.

2.3.2.5 Conclusion

It should state clearly the main conclusions and include the explanation of their relevance or importance to the field.

2.3.3 Back Matter

2.3.3.1 Acknowledgments

Anyone who contributed towards the article but does not meet the criteria for authorship, including those who provided professional writing services or materials, should be acknowledged. Authors should obtain permission to acknowledge from all those mentioned in the Acknowledgments section. This section is not added if the author does not have anyone to acknowledge.

2.3.3.2 Authors' Contributions

Each author is expected to have made substantial contributions to the conception or design of the work, or the acquisition, analysis, or interpretation of data, or the creation of new software used in the work, or have drafted the work or substantively revised it.

Please use Surname and Initial of Forename to refer to an author's contribution. For example: made substantial contributions to conception and design of the study and performed data analysis and interpretation: Salas H, Castaneda WV; performed data acquisition, as well as provided administrative, technical, and material support: Castillo N, Young V.

If an article is single-authored, please include "The author contributed solely to the article." in this section.

2.3.3.3 Availability of Data and Materials

In order to maintain the integrity, transparency and reproducibility of research records, authors should include this section in their manuscripts, detailing where the data supporting their findings can be found. Data can be deposited into data repositories or published as supplementary information in the journal. Authors who cannot share their data should state that the data will not be shared and explain it. If a manuscript does not involve such issue, please state "Not applicable." in this section.

2.3.3.4 Financial Support and Sponsorship

All sources of funding for the study reported should be declared. The role of the funding body in the experiment design, collection, analysis and interpretation of data, and writing of the manuscript should be declared. Any relevant grant numbers and the link of funder's website should be provided if any. If the study is not involved with this issue, state "None." in this section.

2.3.3.5 Conflicts of Interest

Authors must declare any potential conflicts of interest that may be perceived as inappropriately influencing the representation or interpretation of reported research results. If there are no conflicts of interest, please state "All authors declared that there are no conflicts of interest." in this section. Some authors may be bound by confidentiality agreements. In such cases, in place of itemized disclosures, we will require authors to state "All authors declare that they are bound by confidentiality agreements that prevent them from disclosing their conflicts of interest in this work.". If authors are unsure whether conflicts of interest exist, please refer to the "Conflicts of Interest" of *EVCNA* Editorial Policies for a full explanation.

2.3.3.6 Ethical Approval and Consent to Participate

Research involving human subjects, human material or human data must be performed in accordance with the Declaration of Helsinki and approved by an appropriate ethics committee. An informed consent to participate in the study should also be obtained from participants, or their parents or legal guardians for children under 16. A statement detailing the name of the ethics committee (including the reference number where appropriate) and the informed consent obtained must appear in the manuscripts reporting such research.

Studies involving animals and cell lines must include a statement on ethical approval. More information is available at Editorial Policies.

If the manuscript does not involve such issue, please state "Not applicable." in this section.

2.3.3.7 Consent for Publication

Manuscripts containing individual details, images or videos, must obtain consent for publication from that person, or in the case of children, their parents or legal guardians. If the person has died, consent for publication must be obtained from the next of kin of the participant. Manuscripts must include a statement that a written informed consent for publication was obtained. Authors do not have to submit such content accompanying the manuscript. However, these documents must be available if requested. If the manuscript does not involve this issue, state "Not applicable." in this section.

2.3.3.8 Copyright

Authors retain copyright of their works through a Creative Commons Attribution 4.0 International License that clearly states how readers can copy, distribute, and use their attributed research, free of charge. A declaration "© The Author(s) 2021." will be added to each article. Authors are required to sign License to Publish before formal publication.

2.3.3.9 References

Preferably original research articles that directly support the statements should be cited. Review articles could be cited when they specifically address the statement made in the manuscript. An abstract should not be used as a reference. Non-specific citations should be avoided.

References should be numbered in order of appearance at the end of manuscripts. In the text, reference numbers should be placed in square brackets and the corresponding references are cited thereafter. If the number of authors is less than or equal to six, we require to list all authors' names. If the number of authors is more than six, only the first three authors' names are required to be listed in the references, other authors' names should be omitted and replaced with "et al.". Abbreviations of the journals should be provided on the basis of Index Medicus. Information from manuscripts accepted but not published

should be cited in the text as "Unpublished material" with written permission from the source.

Types	Examples
Journal articles by individual authors	Weaver DL, Ashikaga T, Krag DN, et al. Effect of occult metastases on survival in node-negative breast cancer. *N Engl J Med* 2011;364:412-21. [PMID: 21247310 DOI: 10.1056/NEJMoa1008108]
Organization as author	Diabetes Prevention Program Research Group. Hypertension, insulin, and proinsulin in participants with impaired glucose tolerance. *Hypertension* 2002;40:679-86. [PMID: 12411462]
Both personal authors and organization as author	Vallancien G, Emberton M, Harving N, van Moorselaar RJ; Alf-One Study Group. Sexual dysfunction in 1,274 European men suffering from lower urinary tract symptoms. *J Urol* 2003;169:2257-61. [PMID: 12771764 DOI: 10.1097/01.ju.0000067940.76090.73]
Journal articles not in English	Zhang X, Xiong H, Ji TY, Zhang YH, Wang Y. Case report of anti-N-methyl-D-aspartate receptor encephalitis in child. *J Appl Clin Pediatr* 2012;27:1903-7. (in Chinese)
Journal articles ahead of print	Odibo AO. Falling stillbirth and neonatal mortality rates in twin gestation: not a reason for complacency. BJOG 2018; Epub ahead of print [PMID: 30461178 DOI: 10.1111/1471-0528.15541]
Books	Sherlock S, Dooley J. Diseases of the liver and billiary system. 9th ed. Oxford: Blackwell Sci Pub; 1993. pp. 258-96.
Book chapters	Meltzer PS, Kallioniemi A, Trent JM. Chromosome alterations in human solid tumors. In: Vogelstein B, Kinzler KW, editors. The genetic basis of human cancer. New York: McGraw-Hill; 2002. pp. 93-113.
Online resource	FDA News Release. FDA approval brings first gene therapy to the United States. Available from: https://www.fda.gov/NewsEvents/Newsroom/PressAnnouncements/ucm574058.htm. [Last accessed on 30 Oct 2017]
Conference proceedings	Harnden P, Joffe JK, Jones WG, editors. Germ cell tumours V. Proceedings of the 5th Germ Cell Tumour Conference; 2001 Sep 13-15; Leeds, UK. New York: Springer; 2002.
Conference paper	Christensen S, Oppacher F. An analysis of Koza's computational effort statistic for genetic programming. In: Foster JA, Lutton E, Miller J, Ryan C, Tettamanzi AG, editors. Genetic programming. EuroGP 2002: Proceedings of the 5th European Conference on Genetic Programming; 2002 Apr 3-5; Kinsdale, Ireland. Berlin: Springer; 2002. pp. 182-91.
Unpublished material	Tian D, Araki H, Stahl E, Bergelson J, Kreitman M. Signature of balancing selection in Arabidopsis. *Proc Natl Acad Sci U S A*. Forthcoming 2002.

For other types of references, please refer to U.S. National Library of Medicine.
The journal also recommends that authors prepare references with a bibliography software package, such as EndNote to avoid typing mistakes and duplicated references.

2.3.3.10 Supplementary Materials

Additional data and information can be uploaded as Supplementary Materials to accompany the manuscripts. The supplementary materials will also be available to the referees as part of the peer-review process. Any file format is acceptable, such as data sheet (word, excel, csv, cdx, fasta, pdf or zip files), presentation (powerpoint, pdf or zip files), image (cdx, eps, jpeg, pdf, png or tiff), table (word, excel, csv or pdf), audio (mp3, wav or wma) or video (avi, divx, flv, mov, mp4, mpeg, mpg or wmv). All information should be clearly presented. Supplementary materials should be cited in the main text in numeric order (e.g., Supplementary Figure 1, Supplementary Figure 2, Supplementary Table 1, Supplementary Table 2, *etc.*). The style of supplementary figures or tables complies with the same requirements on figures or tables in main text. Videos and audios should be prepared in English and limited to a size of 500 MB.

2.4 Manuscript Format

2.4.1 File Format

Manuscript files can be in DOC and DOCX formats and should not be locked or protected.

2.4.2 Length

There are no restrictions on paper length, number of figures, or amount of supporting documents. Authors are encouraged to present and discuss their findings concisely.

2.4.3 Language

Manuscripts must be written in English.

2.4.4 Multimedia Files

The journal supports manuscripts with multimedia files. The requirements are listed as follows:
Videos or audio files are only acceptable in English. The presentation and introduction should be easy to understand. The frames should be clear, and the speech speed should be moderate.
A brief overview of the video or audio files should be given in the manuscript text.
The video or audio files should be limited to a size of up to 500 MB.
Please use professional software to produce high-quality video files, to facilitate acceptance and publication along with the

submitted article. Upload the videos in mp4, wmv, or rm format (preferably mp4) and audio files in mp3 or wav format.

2.4.5 Figures

Figures should be cited in numeric order (e.g., Figure 1, Figure 2) and placed after the paragraph where it is first cited;
Figures can be submitted in format of tiff, psd, AI or jpeg, with resolution of 300-600 dpi;
Figure caption is placed under the Figure;
Diagrams with describing words (including, flow chart, coordinate diagram, bar chart, line chart, and scatter diagram, *etc.*) should be editable in word, excel or powerpoint format. Non-English information should be avoided;
Labels, numbers, letters, arrows, and symbols in figure should be clear, of uniform size, and contrast with the background;
Symbols, arrows, numbers, or letters used to identify parts of the illustrations must be identified and explained in the legend;
Internal scale (magnification) should be explained and the staining method in photomicrographs should be identified;
All non-standard abbreviations should be explained in the legend;
Permission for use of copyrighted materials from other sources, including re-published, adapted, modified, or partial figures and images from the internet, must be obtained. It is authors' responsibility to acquire the licenses, to follow any citation instruction requested by third-party rights holders, and cover any supplementary charges.

2.4.6 Tables

Tables should be cited in numeric order and placed after the paragraph where it is first cited;
The table caption should be placed above the table and labeled sequentially (e.g., Table 1, Table 2);
Tables should be provided in editable form like DOC or DOCX format (picture is not allowed);
Abbreviations and symbols used in table should be explained in footnote;
Explanatory matter should also be placed in footnotes;
Permission for use of copyrighted materials from other sources, including re-published, adapted, modified, or partial tables from the internet, must be obtained. It is authors' responsibility to acquire the licenses, to follow any citation instruction requested by third-party rights holders, and cover any supplementary charges.

2.4.7 Abbreviations

Abbreviations should be defined upon first appearance in the abstract, main text, and in figure or table captions and used consistently thereafter. Non-standard abbreviations are not allowed unless they appear at least three times in the text. Commonly-used abbreviations, such as DNA, RNA, ATP, *etc*., can be used directly without definition. Abbreviations in titles and keywords should be avoided, except for the ones which are widely used.

2.4.8 Italics

General italic words like *vs*., *et al., etc*., *in vivo*, *in vitro*; *t* test, *F* test, *U* test; related coefficient as *r*, sample number as *n*, and probability as *P*; names of genes; names of bacteria and biology species in Latin.

2.4.9 Units

SI Units should be used. Imperial, US customary and other units should be converted to SI units whenever possible. There is a space between the number and the unit (i.e., 23 mL). Hour, minute, second should be written as h, min, s.

2.4.10 Numbers

Numbers appearing at the beginning of sentences should be expressed in English. When there are two or more numbers in a paragraph, they should be expressed as Arabic numerals; when there is only one number in a paragraph, number < 10 should be expressed in English and number > 10 should be expressed as Arabic numerals. 12345678 should be written as 12,345,678.

2.4.11 Equations

Equations should be editable and not appear in a picture format. Authors are advised to use either the Microsoft Equation Editor or the MathType for display and inline equations.

2.5 Submission Link

Submit an article via https://oaemesas.com/login?JournalId=evcna.

www.oaepublish.com

Extracellular Vesicles and Circulating Nucleic Acids (*EVCNA*)
Los Angeles Office
245 E Main Street ste122, Alhambra,
CA 91801, USA
E-mail: editorial@evcna.com
Website: https://evcna.com